

AD-A111 097

AIR FORCE INST OF TECH WRIGHT-PATTERSON AFB OH SCHOOL--ETC F/8 6/16
THE INFLUENCE OF SURGICAL HERNIATION ON THE VISCOELASTIC PROPER--ETC(U)
DEC 88 D R FURLONG
AFIT/0AE/AA/81D-9

UNCLASSIFIED

NL

for 1
26
3/11/007

END
DATE
FILMED
6-82
DTIC

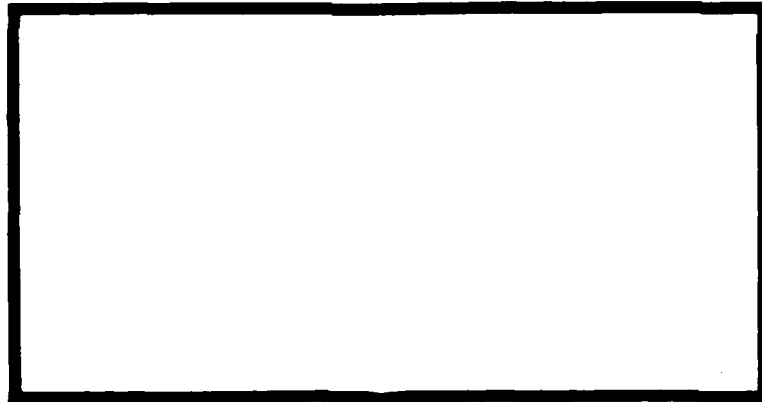
AD A111097

LEVEL II

①



STG
 FEB 13 1982
 S



DTC FILE COPY

UNITED STATES AIR FORCE
 AIR UNIVERSITY
 AIR FORCE INSTITUTE OF TECHNOLOGY
 Wright-Patterson Air Force Base, Ohio

This document has been approved
 for public release and sale; its
 distribution is unlimited.

82 02 18 056

AFIT/GAE/AA/81D-9

THE INFLUENCE OF SURGICAL HERNIATION
ON THE VISCOELASTIC PROPERTIES
OF THE INTERVERTEBRAL JOINT
THESIS

AFIT/GAE/AA/81D-9 David R. Furlong

ACKNOWLEDGEMENTS

I would like to thank Professor A. N. Palazotto for his technical help, knowledge, advice, and concern. I would also like to thank Lt E. Paul France of the Air Force Aerospace Medical Research Laboratory for his help during the experimentation and the analysis. Thanks also to Capt Ron L. Hinrichsen for his assistance in my computer work.

A special thanks to my mother and father for encouraging me to apply to AFIT in my last year at Georgia Tech.

David R. Furlong

CONTENTS

Acknowledgements.....	ii
Contents.....	iii
List of Figures.....	v
List of Symbols.....	vii
Abstract.....	ix
1. Introduction.....	1
1.1 Background.....	1
1.2 Purpose.....	2
1.3 Anatomy.....	3
1.4 Assumption and General Approach.....	7
2. Experimentation.....	8
2.1 Introduction.....	8
2.2 Consideration.....	8
2.3 Protocol.....	12
2.4 Results.....	15
3. Viscoelastic Theory.....	20
3.1 Introduction.....	20
3.2 One Dimensional Viscoelastic Theory.....	20
3.3 Three Dimensional Viscoelastic Theory.....	22
3.4 Elastic Analysis.....	24
3.5 Viscoelastic Analysis.....	26
4. Finite Element Analysis of Experimental Data.....	30
4.1 Introduction.....	30
4.2 Formulation of Model.....	30
4.3 Course Mesh Analysis.....	34

4.4	Fine Mesh Analysis.....	35
4.4.1	Analysis of the Healthy Specimen.....	39
4.4.2	Analysis of the Fully Herniated Specimen.....	40
4.4.3	Analysis of the Osteo Specimen.....	50
4.4.4	Comparison of Analytical Results.....	57
5.	Conclusions.....	65
	Bibliography.....	67
	Appendix A Experimental Protocol.....	69

List of Figures

1.1	Rhesus Monkey Vertebral Column.....	4
1.2	Vertebral Unit With Posterior Element.....	5
1.3	Disc Region.....	5
1.4	Cut-Away of Vertebral Unit.....	6
2.1	Examples of Pitch and Torsion.....	10
2.2	Prepared Specimen.....	11
2.3	Test Chamber.....	14
2.4	Experimental Results of First and Second Test.....	17
2.5	Experimental Results of Fully Herniated Specimen.....	18
2.6	Experimental Results of Osteo Specimen.....	19
3.1	Triangular Element.....	28
3.2	Flow Chart of Finite Element Program.....	29
4.1	Three-Parameter Kelvin Solid.....	31
4.2	Top View of Centrum.....	31
4.3	Coarse Mesh Model.....	35
4.4	Relation of Fine to Coarse Mesh Material Constants.....	36
4.5	Fine Mesh Model.....	39
4.6	Fine Mesh Solution of Healthy Specimen of Vertical Displacement.....	41
4.7	Fine Mesh Solution of Healthy Specimen Radial Displacement.....	42
4.8	Fine Finite Model of Healthy Specimen $t=0^-$	43
4.9	Fine Finite Model of Healthy Specimen $t=0^+$ sec.....	44
4.10	Fine Finite Model of Healthy Specimen $t=1500$ sec.....	45
4.11	Hoop Stress vs. Radius in Centrum.....	46
4.12	Healthy Specimen Radial Stress vs. Radius in Disc.....	47
4.13	Healthy Specimen of Vertical Stress in Disc.....	48

4.14	Healthy Specimen of Hoop Stress in Disc.....	49
4.15	Finite Element Solution of Fully Herniated Specimen.....	51
4.16	Finite Element Model $t=0^+$ of Fully Herniated.....	52
4.17	Finite Element Model $t=1500$ of Fully Herniated.....	53
4.18	Radial Stress vs. Radius in Disc of Fully Herniated Specimen....	54
4.19	Vertical Stress vs. Radius in Disc of Fully Herniated Specimen..	55
4.20	Hoop Stress vs. Radius in Disc of Fully Herniated Specimen.....	56
4.21	Finite Element Solution of Osteo Specimen.....	58
4.22	Finite Element Model of Osteo $t=0^+$ s.	59
4.23	Finite Element Model of Osteo $t=830$ sec.....	60
4.24	Radial Stress vs. Radius in Disc of Osteo Specimen.....	61
4.25	Vertical Stress vs. Radius in Disc of Osteo Specimen.....	62
4.26	Theta Stress vs. Radius in Disc of Osteo Specimen.....	63

List of Symbols

($\dot{\quad}$)	Time Derivative of ()
($\bar{\quad}$)	Mean of ()
a_i	$r_i z_k - r_k z_i$
[A]	Poisson's Ratio Matrix
A_m	Area of Element m
b_i	$r_k - r_i$
[B]	Shape Function Matrix
c_i	$z_i - z_k$
cm	Centimeter
[D]	Elastic Material Property Matrix
dVo	Differential of Original Volume
E	Modulus of Elasticity
e	Component of Strain Dilatation Matrix
e_{ij}	ij Component of Strain Distortion Matrix at Constant Volume
[K]	Elastic Stiffness Matrix
Kp	Kiloponds = 9.8 Newtons
Kp/cm^2	Kiloponds per Square Centimeter
m	Number of Elements
P	Polynomial Operator
p	Polynomial Operator Coefficient
$\{P\}$	Applied Load Matrix
Q	Polynomial Operator
q	Polynomial Operator Coefficient
q_0	Spring Constant in a Kelvin Solid

q_1	Dashpot Constant in a Kelvin Solid
$\{Q\}$	Residual Strain Matrix
r_i	Radius of Node i
S	Component of Dilatation Stress Matrix
S_{ij}	ij Component of the Stress Distortion Matrix at Constant Volume
$\{U\}$	Nodal Displacement Matrix
Z_i	Height of Node i
ϵ^E	Elastic Strain
$\{\epsilon_0\}$	Initial Strain Matrix
ϵ^{VE}	Viscoelastic Strain
ϵ	Strain
ϵ_i	Strain in the i Direction
ϵ_{ij}	ij Component of the Strain
η	Dashpot Constant
σ	Stress
σ_{ij}	ij Component of Stress
τ_{ij}	ij Component of Shear Stress

ABSTRACT

In the phenomena of aircraft flight, the body is subjected to forces and stress that are not ordinarily encountered. Examples are emergency egress from aircraft, high G turns, and the random vibrations and disturbances. Anatomically the vertebral column must absorb much of these excesses. In light of these biomechanics problems of flight, this thesis will study the influence of surgical herniation on the viscoelastic properties of the intervertebral joint. The presentation shall be broken down into two phases: experimentation and analysis.

The experimentation involved several distinct phases. First five specimens were excised from the L₁-L₂ level of young adult rhesus monkeys (*Macaca mulatta*). The prepared specimen consisted of the intervertebral joint and the two adjacent vertebral centrum without either the posterior elements or associated soft tissues. The prepared specimen was subjected to a constant compressive load of sixty-seven newtons for eight hours followed by a relaxation time of sixteen hours. The specimens were then subjected to various stages of herniation and the creep tests were repeated after each herniation.

The analysis was also carried out in several phases. First the experimental data was graphed using a specially prepared plotting routine for the Cyber 750 machine. A mean displacement curve was then obtained for each set of creep tests by averaging the displacement vs. time curve of each test phase. Next, all specimens were dissected and measured to obtain data needed in formulating a finite element model. In the final phase of the analysis, a viscoelastic axisymmetric finite element model was used to quantify the experimental data. A three parameter Kelvin

solid was employed in the finite element solution method. The result of this paper will be used to construct a dynamic model of the vertebral column.

CHAPTER 1

INTRODUCTION

1.1. Background

Numerous studies of the intervertebral disc of both an experimental and an analytical nature have been done. Although the work presented here was done on the rhesus monkey (*Macaca mulatta*), numerous comparisons and correlations can be made between it and those made on human specimens. Work done by Kazarian (8) addresses the specific subject of comparisons between different species.

Several experimental papers have been concerned with the fact that under some loading conditions the intervertebral disc behaves in a viscoelastic manner. Several of the early papers studying the time dependent observation can be attributed to Virgin (17) and Hirsch (7). Markolf (15) considered several cyclic loads on discs in varying states of surgical herniation and always found the disc to behave viscoelastically. More recently, people have been concerned not only with experimentation but also with analysis of the data either by modeling of the results or by altering the specimen and reperforming the experiment. Lin and Liu

(14) considered several types of loading patterns and concluded that during pure axial loading the posterior elements play a minor role in load bearing. Nachemson (16) felt that a grossly herniated disc did not exhibit a significantly different response from the healthy specimens. Kazarian (11), who did numerous compressive tests, concluded that under certain conditions the disc would not behave in a viscoelastic manner.

Although the experimental studies showed viscoelastic phenomena, the analytical methods approach modeling from a variety of viewpoints. Belytschko did an axisymmetric finite element analysis using an orthotropic annulus fibrosus with an incompressible, inviscid nucleus pulposus. Kulak (12) has also done nonlinear modeling using finite elements. He did his work based on analysis by Fung (5) which stated that stress in some biological materials can be broken down into an elastic and history dependent part. Lin (13) did a three dimensional finite element model assuming orthotropic material properties for the disc and vertebrae. Burns (3) discusses the idea of viscoelastic modeling using Kelvin solid units and came to the conclusion that the three-unit solid results in the best quantitative results. Hinrichsen (6) employed an axisymmetric viscoelastic finite element model using a three parameter Kelvin solid.

1.2 Purpose

In aircraft flight, the body can be subjected to severe physical loads; emergency egress, high G turns, and random vibrations. The vertebral column must absorb much of this loading. As a result, intervertebral disc herniation sometimes occurs. In this light, this thesis will investigate the influence of surgical herniation on the

viscoelastic properties of the intervertebral disc. Both experimental and analytical phases will be carried out in this study.

1.3 Anatomy

A brief discussion of rhesus monkey spinal anatomy will be helpful in understanding the remainder of this thesis. First, the gross anatomy of the spine will be examined followed by a more specific discussion of the vertebral segment.

The vertebral column is divided into thirty-three vertebrae: 7 cervical, 12 thoracic, 7 lumbar, 6 sacrum, and 4 coccyx (see fig. (1.1)). In addition, most vertebrae have a disc between two adjacent vertebrae called the intervertebral disc. Several important aspects of the vertebral segment are: posterior elements, longitudinal ligaments, vertebral centrum and disc (see fig. (1.2)).

The concern of this work, however, is mainly in characteristics of the vertebral segment which is made up of two parts: vertebral centrum and intervertebral joint.

The vertebral centrum is composed of three types of hard tissue: cortical bone, trabecular bone, and bony endplate (see fig. (1.4)). The cortical bone is a very thin and strong material which surrounds the outer surface of the centrum. The trabecular bone is a soft material with a matrix very similar to that of sponge. The bony endplate is a hyaline cartilage structure that separates the disc from the centrum.

The disc also has several components: nucleus pulposus and annulus fibrosis (see fig. (1.3)). The nucleus makes up approximately half of the planar cross-section of the disc and is composed of fibrous strands in

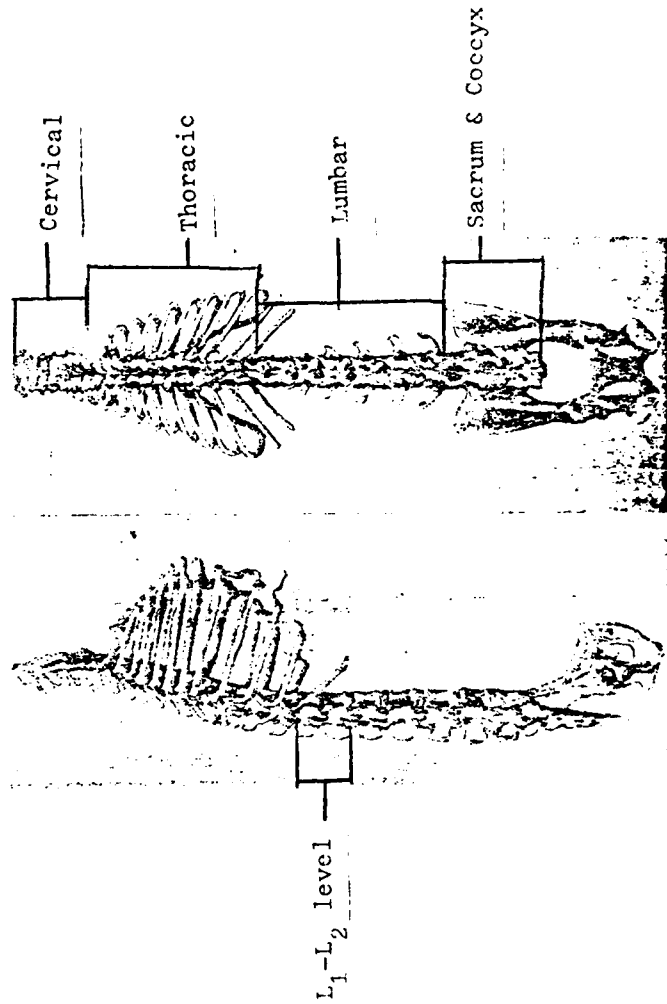


fig. 1.1 (from 8) Sagittal and posterior views of the rhesus monkey vertebral unit.

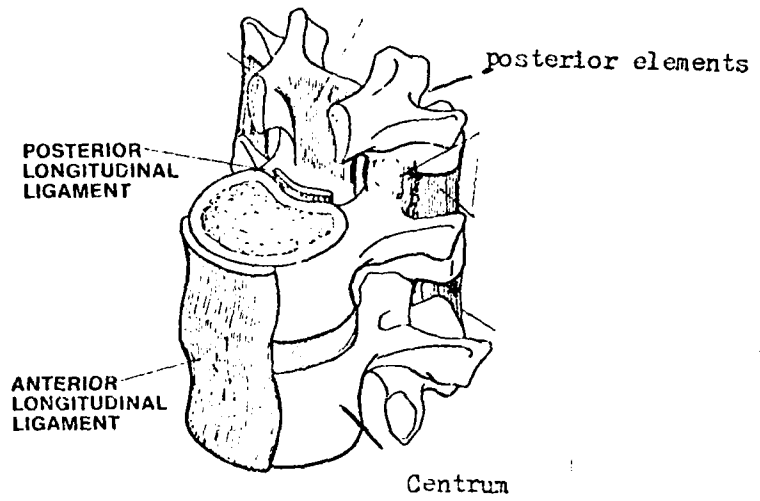


fig. 1.2 (from 18) View of vertebral unit with posterior elements attached.

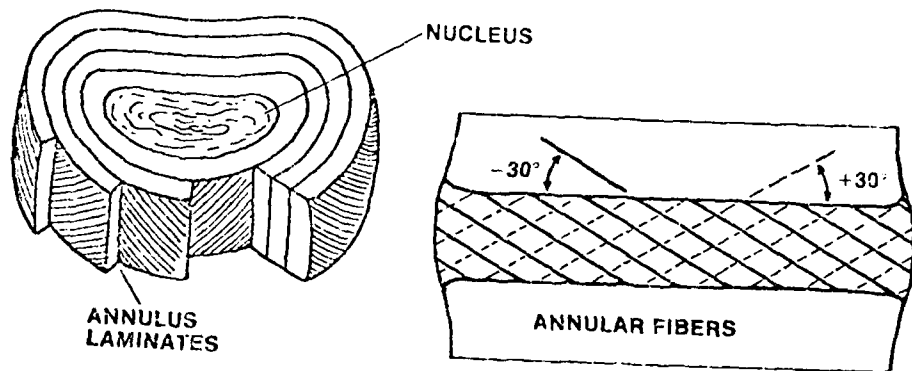


fig. 1.3 A good illustration of the complexity of the disc region

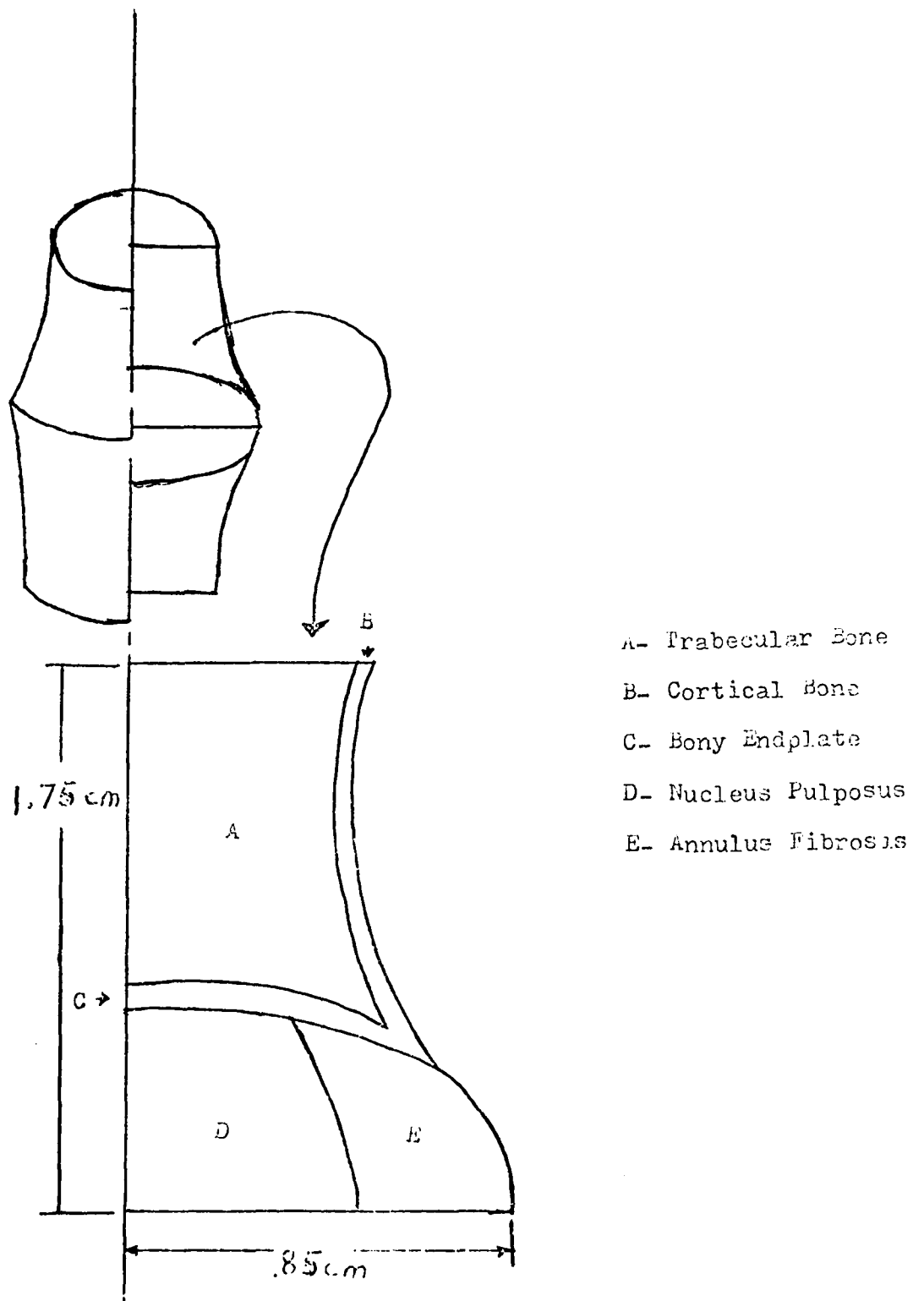


fig. 1.4 A cut-away view of the vertebral unit.

a muco-protein gel with a water content of 70-90%. The annulus is a relatively complicated structure. It consists of fibrous tissue in concentric laminate bands. All fibers in any one band have the same orientation but opposite to that of its two adjacent bands. An analogous structure to the disc is the jelly donut where the nucleus is the jelly and the annulus serves as the dough.

1.4 Assumptions and General Approach

The general approach of this thesis can be divided into two sections: experimentation and analysis.

The experimentation involved tests of lumbar intervertebral disc at the L_1-L_2 level in varying states of surgical herniation. At all stages of herniation, a creep test was done with an eight-hour compressive load followed by a sixteen-hour relaxation time. The experimental results indicated that the creep behavior of the specimen is not altered unless the disc is grossly herniated.

The analysis of the experimental data was done in the following manner. The specimen was modeled assuming rotational symmetry about the center of the disc. A finite element analysis was done to obtain the material properties of the disc when the disc is modeled as a spring in series with a Kelvin solid. In addition, stress profiles and deformed plots were obtained of the specimen at various times and stages of herniation.

The final conclusion indicated that, in all stages of surgical herniation, the disc behaves in a viscoelastic manner. Moreover, the larger degree of herniation corresponded well with a larger initial displacement and a faster creep rate over time.

CHAPTER 2

EXPERIMENTATION

2.1 Introduction

The primary aspects of the experimentation were: considerations, protocol and results. In the considerations, the experimental data must conform to an established method of analysis. In addition, the experimental protocol must be structured so that all test specimens are tested as equally as possible. A thorough experimental procedure is given in Appendix A.

2.2 Considerations

In determining what types of information were desired from experimentation, several factors had to be considered. These considerations included shape, movement during testing, age and condition, drying out, and method of herniation of the specimen.

Several factors were important in determining shape of the specimen. It should have symmetry with respect to its top and bottom half. In addition, the shape of the specimen must lend itself to an axisymmetric

analysis. These two considerations were satisfied by using the disc at the L_1-L_2 level of the rhesus monkey spine.

Another consideration which the experimentation must meet is the movement of the specimen must be in a purely compressive fusion to insure that an axisymmetric analysis is justified. Two pretests were run on sample specimens to determine if pitch or torsion of the top centrum relative to the bottom centrum occurred (see fig. (2.1) for examples of pitch and torsion). Both pretest specimens displayed pitch and torsion. To insure against the non-vertical movement during the experimentation, each specimen was cupped with a dental acrylic. The cupping also allowed for a more evenly distributed load across the top edge of the test sample. Finally, to measure any pitch or torsion which might have occurred, each specimen had two pins placed in each centrum and time delay photographs were taken to measure the pitch and torsion (see fig. (2.2 and 2.3)).

Age and condition of the specimen were also an important factor before the experimentation. If either of these two varied over a wide range, difficulty could arise in the analysis because both age and condition affect the strength characteristics of the vertebral column. In addition, one could have difficulty in obtaining a mean when these two factors run the gamut. To determine age and condition of each specimen, each vertebral column was X-rayed in the anterior-posterior and the sagittal planes. The age of the specimen was then determined by a veterinarian by measuring the thickness of the epiphyseal plate. All spines were determined to have come from young adult rhesus monkeys. One specimen was found to be diseased and as a result the data gathered from it was not used in obtaining mean displacement curves.

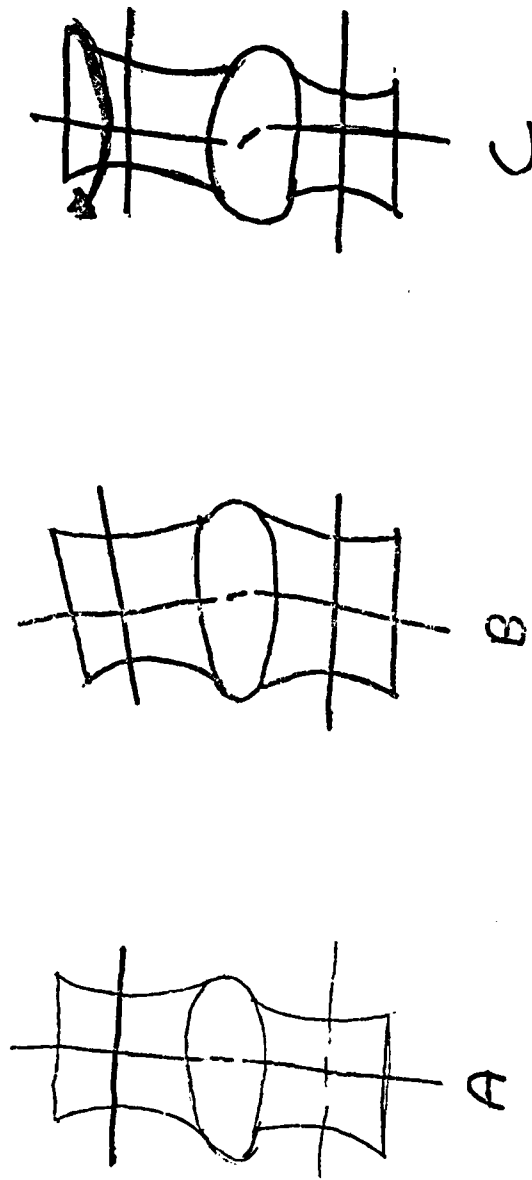


fig. 2.1 The three figures above illustrate the types of movement that can occur in loading of uncapped specimens. "A" illustrates a purely compressive displacement. "B" is a case of the top centrum pitching relative to the bottom centrum. "C" is an example of torsion as is evidenced by the movement of the vertical centerline.

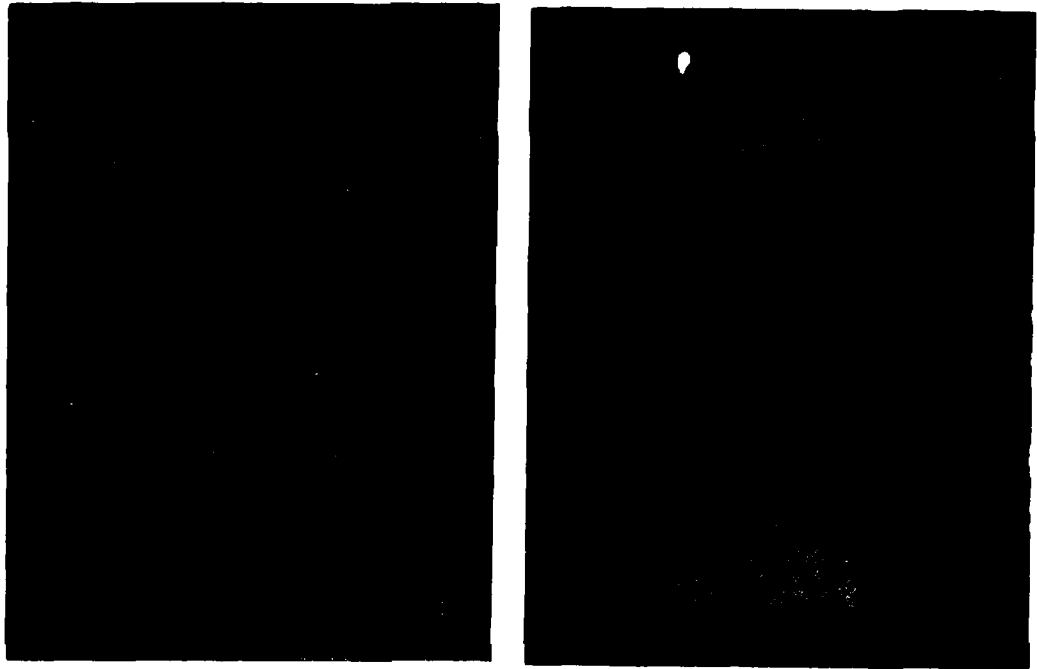


fig 2.2 "A" is a picture of the uncupped prepared specimen. "B" is a view of the cupped specimen ready for testing. Note that both specimens have two pins in each vertebral centrum. These pins are used to measure pitch and torsion from the time delay photographs.

Since the testing was carried out over a period of twenty-four hours, drying out of the specimen was considered. In addition, one is concerned with the specimen absorbing too much fluid because altering water content of the disc has been shown by Anderson (1) to change material properties. To insure against either of these, several steps were taken. First, during the experimentation, the specimen was placed in an environment of approximately 100% relative humidity. And during the storage, the specimens were placed in a saline rich environment and kept refrigerated.

The final concern was determining the method of herniation. Ideally one would like to remove the nucleus pulposus from the disc without altering the annulus fibrosis. In the first attempt at herniation, a hypodermic needle is used to remove the nucleus pulposus. The experimental results, however, indicated no difference from the healthy specimens. In a second attempt to herniate a trephine, a surgical instrument similar in structure to a hole saw, was used to remove a small piece of the annulus and thus negate the nucleus as a structural component of the disc. At that point, it was necessary to make the assumption that as the nucleus passed through the small hole in the annulus, made by the trephine, it contributed to the load resistance in the annulus and thus created no discontinuity.

2.3 Protocol

The experimental protocol was divided into three parts: Preparation, carrying out of load cycles in each stage of herniation, and dissection of the specimen.

Preparation of the specimen involved several steps. The specimen was first removed from the L₁-L₂ level of the vertebral column of young adult rhesus monkeys. Next, all soft tissue was removed from both the centrums and the posterior elements. Care was taken not to damage the disc and the anterior and the posterior longitudinal ligaments. The ligaments were kept intact because to remove them would have resulted in damage to the disc. The final step before cupping of the specimen was to remove the posterior elements. The cupping of each specimen was done with a minimal amount of dental acrylic to insure the cup was not clamped to the specimen and thus possibly create a moment during the loadings. In addition, a special jig was used to insure both cups were set parallel to one another.

The first load cycle involved testing of the healthy specimens. The tests were carried out in specially built humidity chambers to insure the water content of the specimen did not change (see fig. 2.3). The displacement of the top edge of the specimen was recorded through all load-unload cycles with an LVDT (Linear Variable Differential Transducer) whose accuracy was 0.0002 centimeters. In addition, the LVDT was calibrated and set to zero before each loading. Throughout the test, time delay photographs of the specimens were taken every twenty-four seconds to obtain data on pitch, torsion, and bulge data of the disc. After this preparation, the specimens were then subjected to an eight-hour load phase and sixteen-hour unload phase in the test cycle. During the load phase, a total dead weight of 6.7 kiloponds was applied. During the unload, the weight was removed to obtain the relaxation curve.

In the second load cycle, the general procedure was the same as the first except an attempt was made to herniate the disc with fourteen-gauge

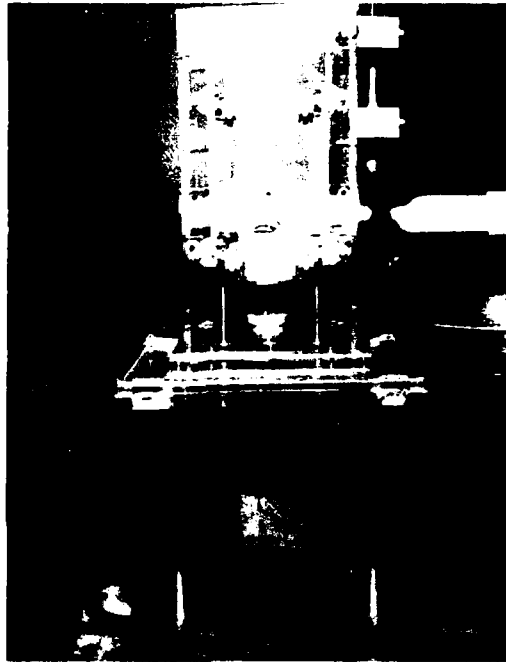


fig. 2.3 Forward view of the test chamber with specimen and dead load.

hypodermic needle. The nucleus was then drawn out using suction.

In the final load cycle, a trephine was used to herniate the disc. In this method, the trephine made a 5mm hole in the annulus allowing the nucleus to flow out through the annulus during the loading.

After the final loading test, all specimens were dissected to obtain measurements needed in formulating the finite element model.

2.4 Results

Not only did the experimental results conform with expectations, but the graphed data gave a clear indication of the method of analysis. In examination of the time delay photographs, all specimens showed a purely compressive displacement with no measurable pitch or torsion. In addition, the disc was shown to bulge two to four percent during the load cycles. The creep curves of displacement versus time in the following pages were established by obtaining the mean of all five specimens over time. The last curve, which shall be referred to as osteo, is that of a diseased specimen and will be examined separately from the other data.

The osteo specimen was diagnosed by a veterinarian to have osteochondritis. From a physical standpoint, this disease may be explained by the fact that the bony endplate extended into the nucleus pulposus to the point where the disc had almost no nucleus pulposus. The value of this specimen lies in comparing its material properties to that of the healthy.

The mean displacement versus time curve for the first two test cycles turned out to be identical (see fig. (2.4)). Several factors con-

tribute to this similarity. When the disc was herniated with the needle, almost no fluid was extracted from nucleus. As a result, one would assume very little or no change in the creep curve. A second reason for the lack of change between the two curves was a self-sealing mechanism proposed by White (18) that states the annulus will reseal itself to prevent escape of the nucleus when the disc is damaged. Because the curve for the first two load cycles was identical, the results from the first herniation shall not be further analyzed. Finally, the mean displacement versus time curve shows the specimens behaved in a viscoelastic manner.

The second experimental curve (see fig. (2.5)) which is the mean curve for those specimens herniated with a trephine shows marked differences from the previous curve. Not only is the initial displacement larger than the healthy specimen, but the grossly herniated one shows a faster creep rate over time. The grossly herniated specimen also displays viscoelastic characteristics over time.

The final curve of the osteo specimen (see fig. (2.6)) is perhaps the most confusing. The creep curve shows a smaller initial displacement than the healthy specimen. In addition, the creep rate for this specimen was faster than that of the healthy. Once again, the displacement versus time for this curve exhibits creep.

The preliminary results to this point are excellent. Even though the first attempt at herniation was not successful, the results were easily explained and understood. Secondly, the curves obtained from this experiment are very similar to those obtained by Virgin (17), Markolf (19), and Nachemson (16). In the next chapter, a viscoelastic theory will be developed to assist in modeling of the data.

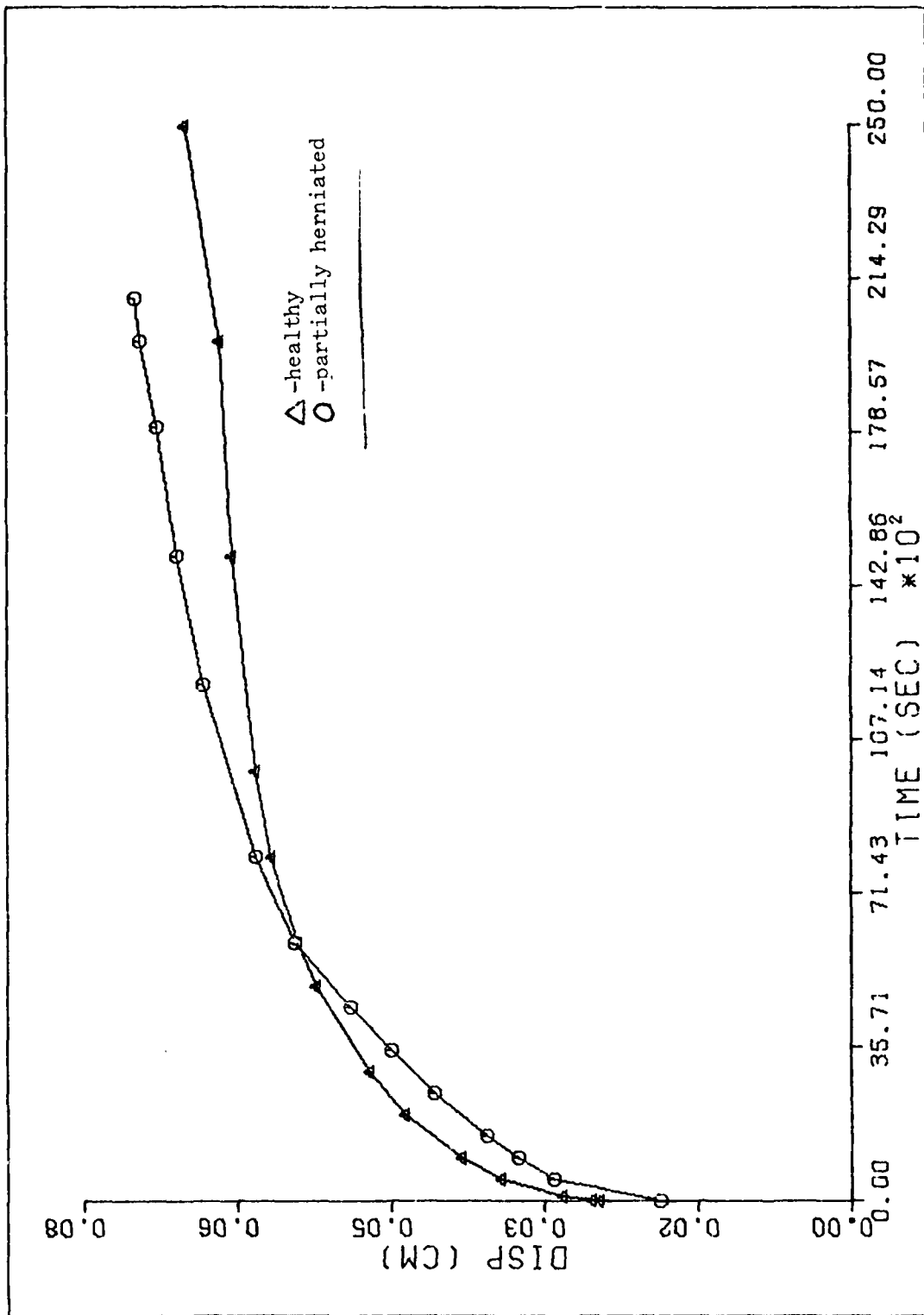


fig.2.4 Experimental results of first two load cycles.

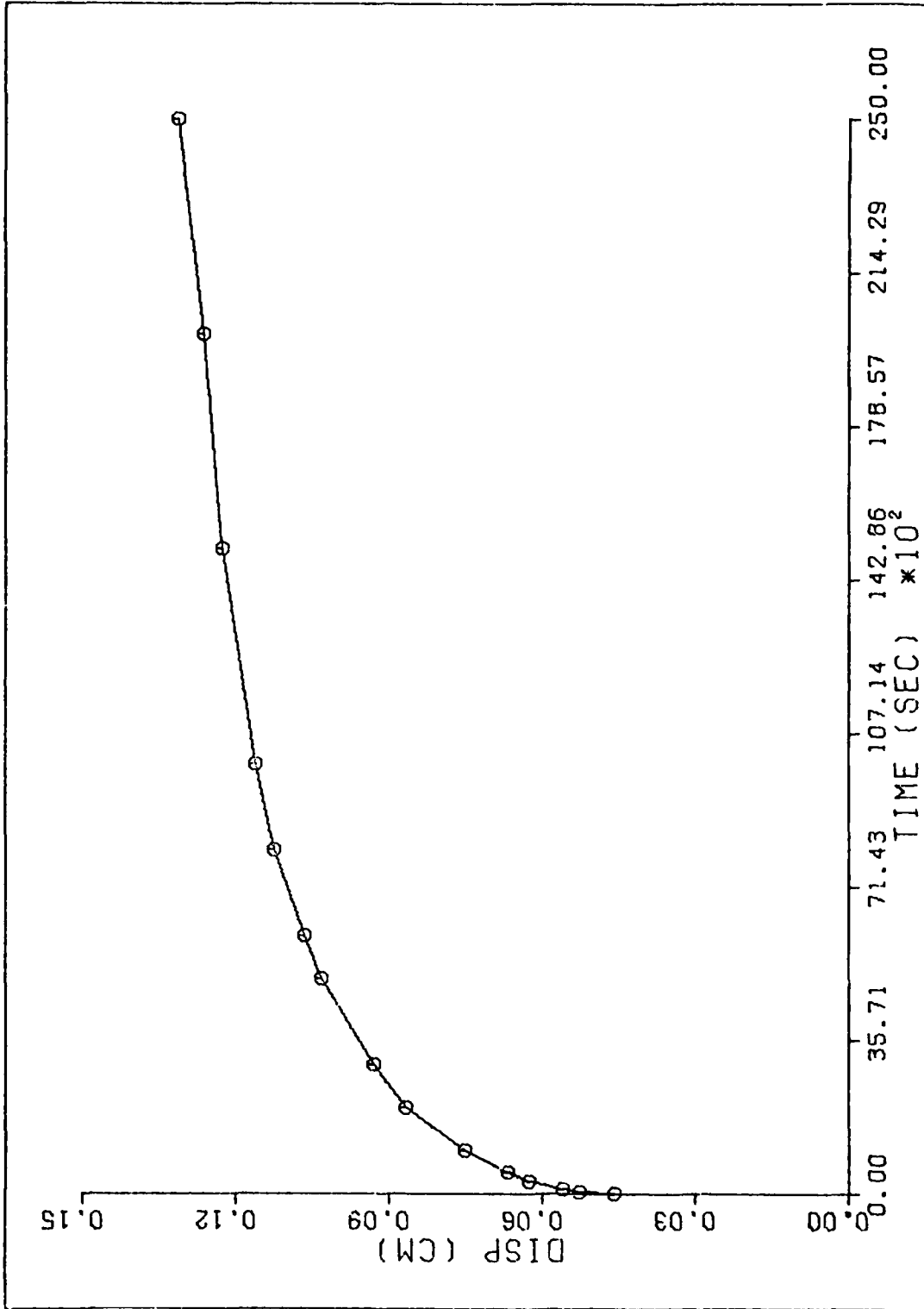


fig. 2.5 Experimental results of fully herniated.

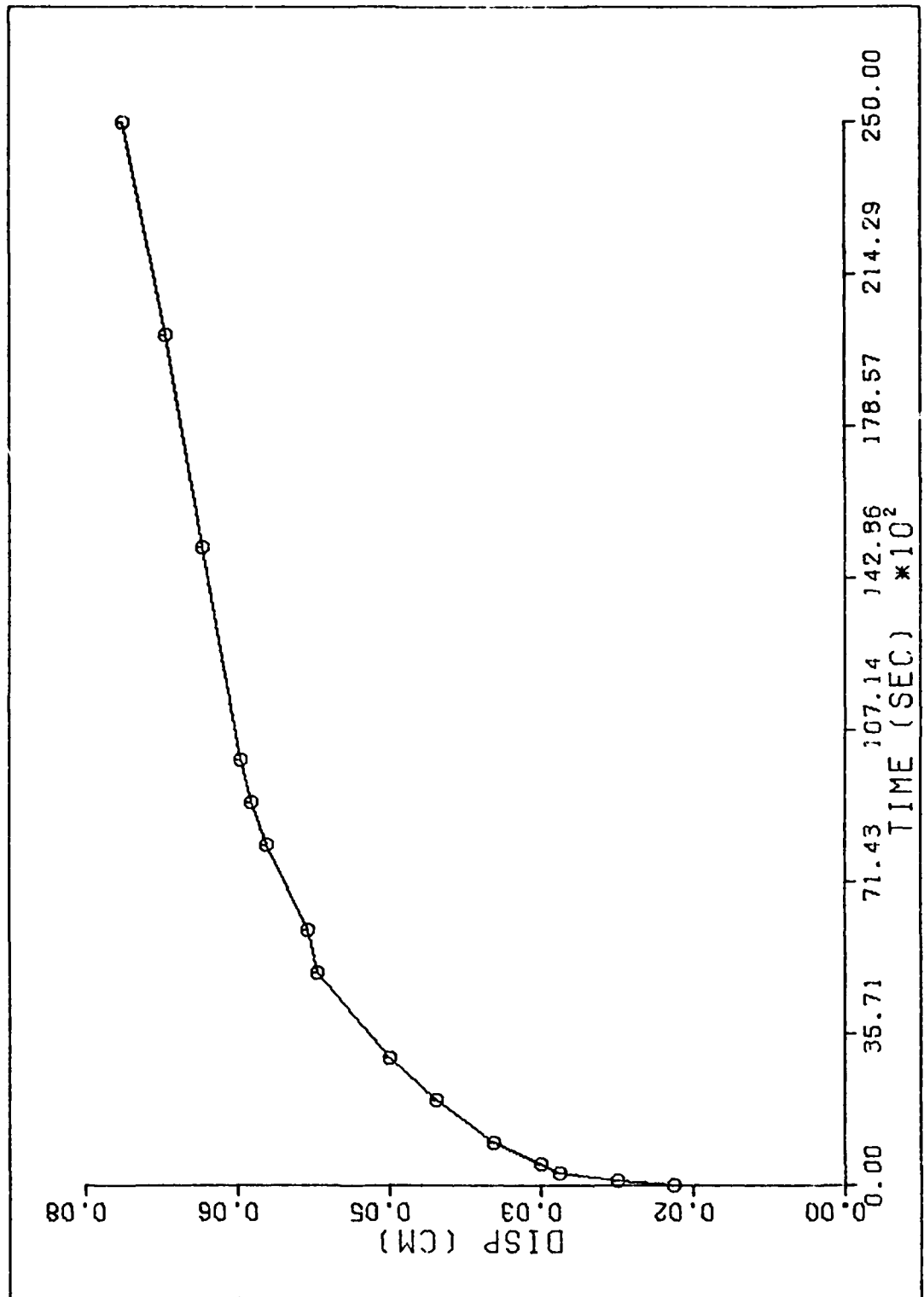


fig. 2.6 Experimental results of the Osteo specimen.

CHAPTER 3

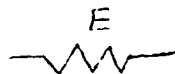
LINEAR VISCOELASTIC THEORY

3.1 Introduction

Viscoelastic theory has been rigorously developed by Flugge (4) and discussed for use in finite element methods by Zienkiewicz (20). The purpose of the following discussion is to give a brief introduction to one and three dimensional viscoelasticity. Finally a finite element formulation of visco elasticity and how it is used in this particular work will be discussed.

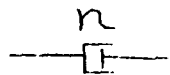
3.2 One Dimensional Viscoelastic Theory

Viscoelasticity models materials using two types of analytical equivalents: spring and dashpots. The spring obeys Hookes law for a stress-strain relation.



$$\sigma = E \epsilon \quad (3-1)$$

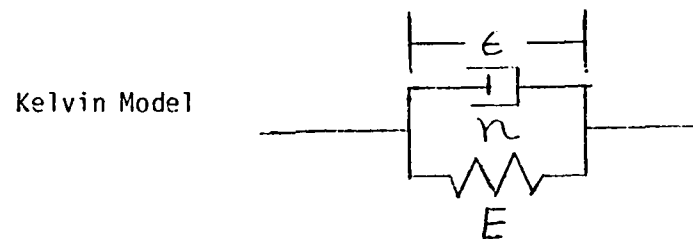
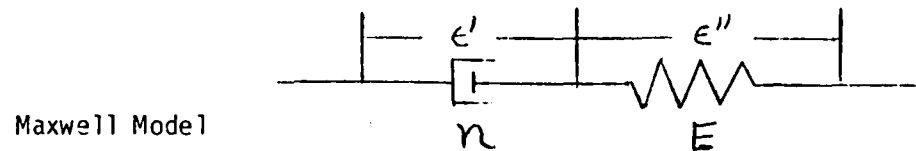
Whereas, the dashpot has a more complex relation for stress-strain.



$$\sigma = n \dot{\epsilon} \quad (3-2)$$

The two units may be combined either in series as a Maxwell model

or in parallel as a Kelvin solid.



The Maxwell model forms on the addition of two strains.

$$\epsilon = \epsilon' + \epsilon'' \quad (3-3)$$

where $\epsilon' = \frac{\delta}{E}$ for spring (3-4)

and $\dot{\epsilon}'' = \frac{\delta}{\eta}$ for dashpot (3-5)

resulting in a constitutive equation

$$\dot{\delta} + p\delta = Q\dot{\epsilon} \quad (3-6)$$

where

$$p = \frac{E}{\eta} \quad Q = E$$

The constitutive equation for the Kelvin solid is developed in an analogous manner based on the sum of two stresses

$$\sigma = \sigma'' + \sigma' \quad (3-7)$$

where $\sigma' = E \epsilon$ for spring (3-8)

and $\sigma'' = \eta \dot{\epsilon}$ for dashpot (3-9)

resulting in the constitutive equation

$$\sigma = \eta \dot{\epsilon} + E \epsilon \quad (3-10)$$

which is now an expression for the creep strain and can now be implemented into the following form

let $\eta = \eta_1$ $E = \eta_0$ $\dot{\epsilon} = \frac{d\epsilon}{dt}$ (3-11, 12)

$$d\epsilon_c = \frac{dt}{\eta_1} \left[\sigma - \eta_0 \epsilon_0 \right] \quad (3-13)$$

3.3 Three-Dimensional Viscoelastic Theory

Three-dimensional viscoelastic theory is based on two ideas: the constitutive equation of one dimensional N Kelvin units model and the viscoelastic law. In a stress analysis of a three-dimensional element, the stress tensor

$$\begin{bmatrix} \sigma_x & \tau_{xy} & \tau_{xz} \\ \tau_{yx} & \sigma_y & \tau_{yz} \\ \tau_{zx} & \tau_{yz} & \sigma_z \end{bmatrix} = \begin{bmatrix} s & 0 & 0 \\ 0 & s & 0 \\ 0 & 0 & s \end{bmatrix} + \begin{bmatrix} s_x & s_{xy} & s_{xz} \\ s_{yx} & s_y & s_{yz} \\ s_{zx} & s_{zy} & s_z \end{bmatrix} \quad (3-14)$$

where

$$s = \frac{1}{3} (\sigma_x + \sigma_y + \sigma_z) \quad (3-15)$$

can be broken down into two components: A trace matrix and a deviatoric matrix. In a similar manner, the strain tensor can be broken into two matrices: dilatation matrix which is volumetric change without change of shape, and a distortion matrix which is change of shape at constant volume.

$$\begin{bmatrix} \epsilon_x & \epsilon_{xy} & \epsilon_{xz} \\ \epsilon_{yx} & \epsilon_y & \epsilon_{yz} \\ \epsilon_{zx} & \epsilon_{zy} & \epsilon_z \end{bmatrix} = \begin{bmatrix} e & 0 & 0 \\ 0 & e & 0 \\ 0 & 0 & e \end{bmatrix} + \begin{bmatrix} e_x & e_y & e_z \\ e_{yx} & e_y & e_{yz} \\ e_{zx} & e_{zy} & e_z \end{bmatrix} \quad (3-16)$$

where

$$e = \frac{1}{3} (e_x + e_y + e_z) \quad (3-17)$$

The first matrix on the right hand side is the dilatation and the second is the distortion matrix.

The viscoelastic law uses the constitutive equation for the Kelvin solid model and the idea of separating the stress and the strain matrices into two components to form a three dimensional viscoelastic equation. If one has an isotropic viscoelastic material, the hydrostatic stress, s , must correspond to a dilatation, e , with no distortion. Using this idea, the following equation is obtained

$$\text{or } \sum_{k=0}^m p_k'' \frac{d^k s}{d\epsilon^k} = \sum_{k=0}^m q_k'' \frac{d^k e}{d\epsilon^k} \quad (3-18)$$

$$p'' s = q'' e \quad (3-19)$$

The second equation from the viscoelastic law yields a relation between the deviatoric stress tensor and the distortion matrix

$$\sum_{k=0}^m p_k' \frac{d^k S}{d\epsilon^k} = \sum_{k=0}^m q_k' \frac{d^k E}{d\epsilon^k} \quad (3-20)$$

or

$$p' S = q' E \quad (3-21)$$

where S & E correspond to the components of the stress and strain deviators. The four operators P'' , Q'' , P' and Q' are entirely independent of one another. In order to find solution to the above equations given a body similar to the intervertebral disc would be extremely difficult if at all possible. For this reason, one is driven to the finite element method.

3.4 Elastic Analysis

The elastic analysis of an axisymmetric problem is divided into several parts. The strain is expressed by (see fig. 3.1 for coordinates)

$$\{\epsilon\} = \begin{Bmatrix} \epsilon_z \\ \epsilon_r \\ \epsilon_\theta \\ \gamma_{rz} \end{Bmatrix} = \begin{Bmatrix} \frac{\partial v}{\partial z} \\ \frac{\partial u}{\partial r} \\ \frac{u}{r} \\ \frac{\partial v}{\partial z} + \frac{\partial u}{\partial r} \end{Bmatrix} \quad (3-22)$$

or in term of the nodal displacement

$$\{\epsilon\} = [B] \{u\} \quad (3-23)$$

where $\{u\}$ is the nodal displacement matrix and $[B]$ is

$$[B] = \frac{1}{2A_m} \begin{bmatrix} 0 & c_i & 0 & c_j & 0 & c_k \\ b_i & 0 & b_j & 0 & b_k & 0 \\ \delta_i & 0 & \delta_j & 0 & \delta_k & 0 \\ c_i & b_i & c_j & b_j & c_k & b_k \end{bmatrix} \quad (3-24)$$

where

$$\delta_i = \frac{a_i}{r} + b_i + c_i \frac{z}{r} \quad (3-25)$$

and A_m is the area of the element.

Similarly the stress is expressed by

$$\{\sigma\} = \begin{Bmatrix} \sigma_z \\ \sigma_r \\ \sigma_\theta \\ \tau_{rz} \end{Bmatrix} = [D] (\{\epsilon\} - \{\epsilon_0\}) \quad (3-26)$$

where $[D]$ is the elastic material property matrix

$$[D] = \frac{E(1-\nu)}{(1+\nu)(1-2\nu)} \begin{bmatrix} 1 & \frac{\nu}{1-\nu} & \frac{\nu}{1-\nu} & 0 \\ & 1 & \frac{\nu}{1-\nu} & 0 \\ & \text{sym} & 1 & 0 \\ & & & \frac{1-2\nu}{2(1-\nu)} \end{bmatrix} \quad (3-27)$$

The overall solution equation to this problem is

$$[K]\{u\} = \{P\} + \{Q\} \quad (3-28)$$

where $[K]$ is the elastic stiffness matrix, $\{P\}$ is the applied load vector, and $\{Q\}$ is the applied load due to initial strains. In integral form, $[K]$ and $\{Q\}$ may be represented as

$$[K] = \sum_{m=1}^M 2\pi \int [B]^T [D] [B] r dr dz \quad (3-29)$$

and

$$\{Q\} = \sum_{m=1}^M 2\pi \int [B]^T [D] \{\epsilon_c\} dV_0 \quad (3-30)$$

The solution method for this problem was formulated assuming a centroidal radius, \bar{r} , and centroidal height, \bar{z} , where

$$\bar{r} = \frac{r_i + r_j + r_k}{3} \quad (3-31)$$

and

$$\bar{z} = \frac{z_i + z_j + z_k}{3} \quad (3-32)$$

The result is a new $[B]$ matrix which shall be referred to as $[\bar{B}]$. At this point one can numerically obtain the stiffness matrix $[K]$ and the residual strain matrix Q without integration. The new expressions for $[K]$ and Q are

$$[K] = \sum_{m=1}^M 2\pi A_m [\bar{B}]^T [D] [B] \bar{r} \quad (3-34)$$

and

$$\{Q\} = \sum_{m=1}^M 2\pi A_m [\bar{B}]^T [D] \{\epsilon_o\} \bar{r} \quad (3-35)$$

At this point, one can obtain the nodal displacements through the solution of equation (3-7).

3.5 Viscoelastic Analysis

The viscoelastic analysis involves the combined concept of elastic strain in addition to the incompressibility of the time dependent characteristics. Thus, the viscoelastic strain can be determined by recognizing that the incorporation of the distortion strain tensor assumes zero volumetric change. The change in volume is contained in the elastic relationships. In order to evaluate the two-dimensional viscoelastic stress, the strain is incrementally determined in the same manner shown in equation (3-13). For the finite element formulation, the strain increment is expressed by

$$\{\Delta \epsilon_c\} = \frac{\Delta t}{\theta_1} \left[\frac{2}{3} [A] \{\dot{\epsilon}\} - \theta_0 \{\epsilon_c\} \right] \quad (3-35)$$

where

$$[A] = \begin{bmatrix} 1 & -\nu_c & -\nu_c & 0 \\ & 1 & -\nu_c & 0 \\ & & 1 & 0 \\ & & & \frac{1-\nu_c}{2} \end{bmatrix} \quad (3-36)$$

In order to use each strain increment $\{\Delta \epsilon_c\}$, the residual strain matrix Q is altered for each time step $\{\Delta t\}$. As a result, one can formulate a viscoelastic problem by using incremental time steps and strain rates. The flow chart for the program used in the analysis is given in fig. 3.2. Thus it is possible with the above equation to incorporate the three

parameter model into the analysis. Therefore, the strain tensor can be written as

$$\epsilon = \epsilon^E + \epsilon^{VE} \quad (3-37)$$

where ϵ^E is the elastic strain tensor which includes volumetric and distortion deformation and ϵ^{VE} is the viscoelastic component for the incompressible strain present in equations (3-35) and (3-36) where $\nu_c = 0.5$.

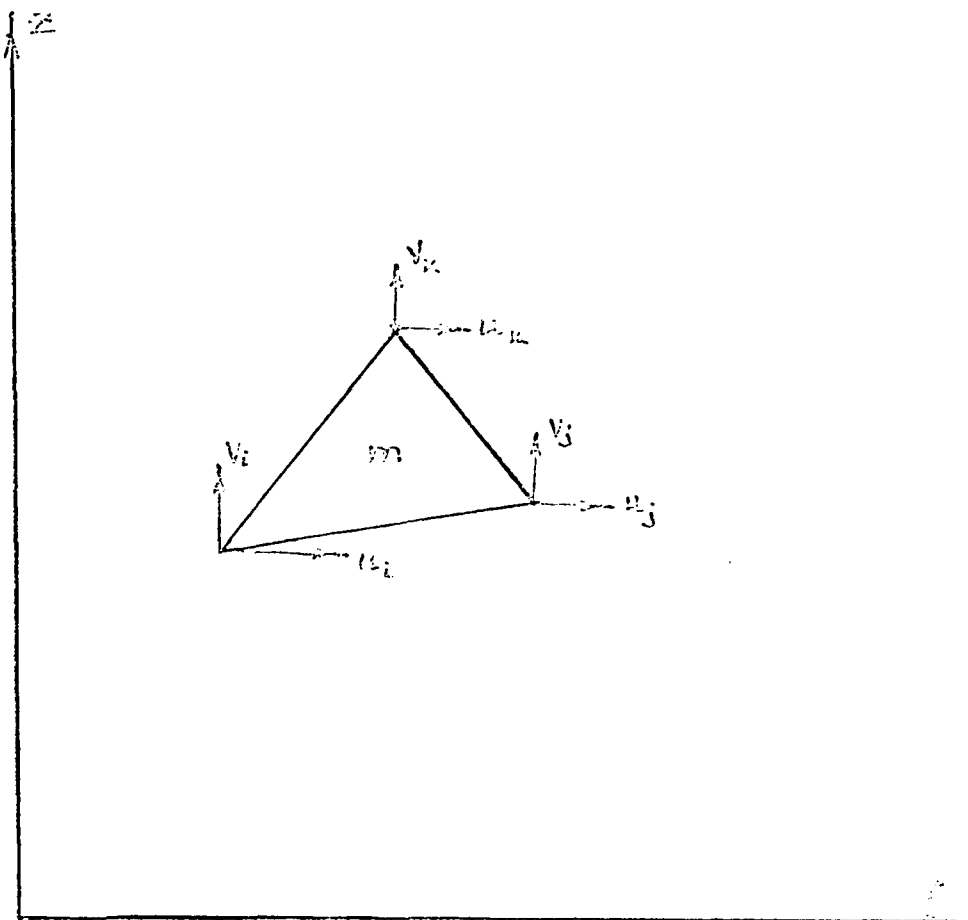


fig 3.1 (from 6) triangular element

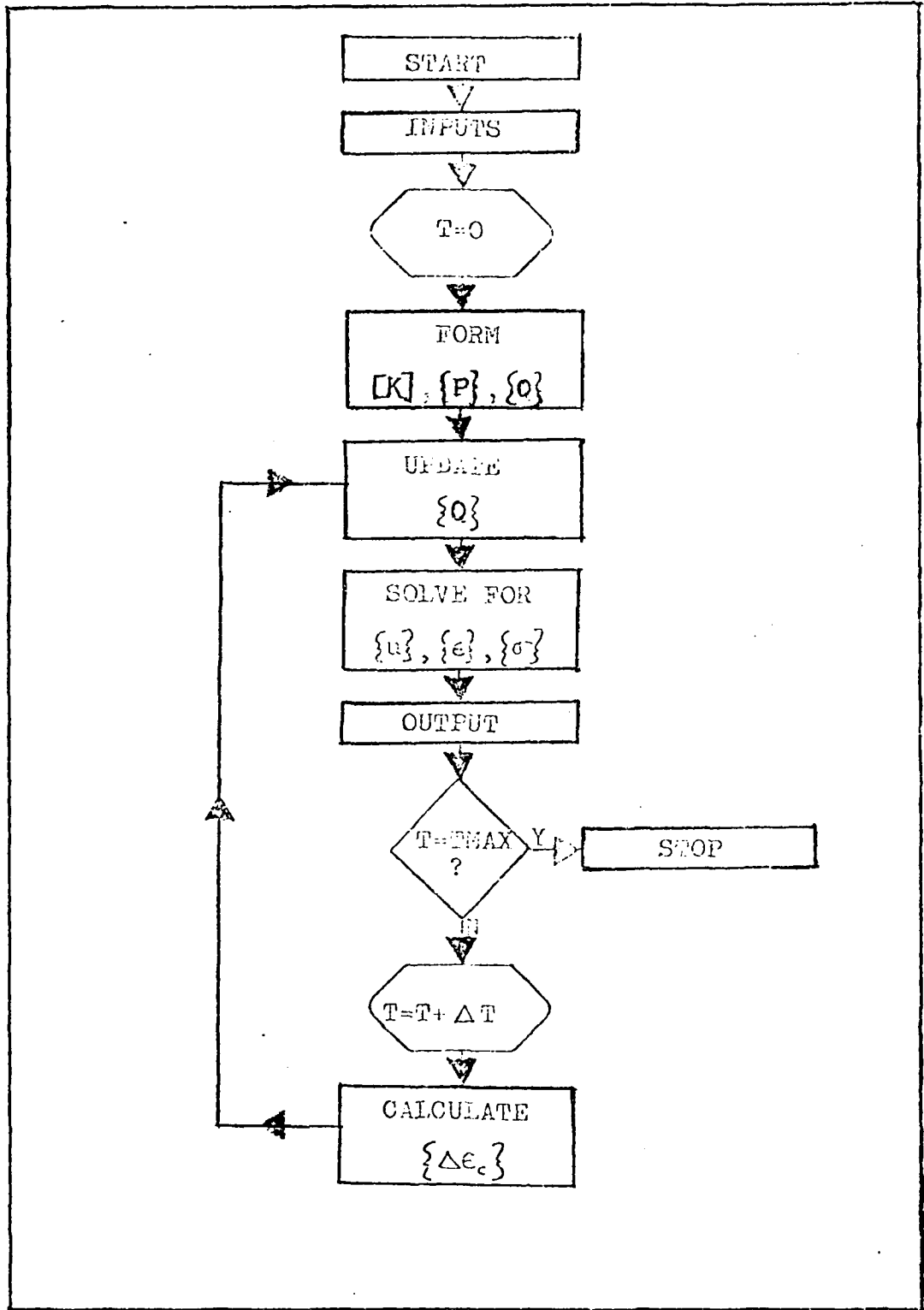


fig. 3.2 (from 6) flow chart of finite element program

CHAPTER 4

FINITE ELEMENT ANALYSIS OF EXPERIMENTAL DATA

4.1 Introduction

The analysis of the experimental data is divided into three parts: formulation of a finite element model, coarse mesh and fine mesh analysis. The three parameter Kelvin solid will be used to model the experimental data (see fig 4.1). The three material constants E_0 , q_0 , and q_1 may be interpreted in the following manner. The elastic spring constant, E_0 is used to match the initial displacement of the specimen. Whereas, the second spring constant, q_0 , determines the displacement over time. The final constant, q_1 , influences the slope of the creep curve.

4.2 Formulation

The formulation of model has three key sections: reasons for an axisymmetric model, modeling of the vertebral centrum and finally modeling of the intervertebral disc.

The axisymmetric analysis is an excellent form of analysis, when studying the intervertebral disc, for several reasons. In a top view of

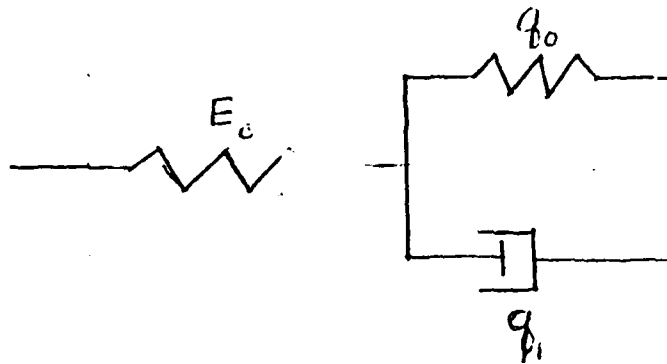


fig. 4.1 A three parameter kelvin solid.



fig. 4.2 The dark line illustrates the shape of the disc from the top. The dotted line is the equivalent circular representation.

the specimen (see fig. (4.2)), the specimen itself is very close to a circle in shape. In addition, the axisymmetric model has been used in the past by several different investigators; Belytschko (2), Kulak (12), and Hinrichsen (6). Finally, this type of analysis enables one to obtain an understanding of the stresses in the disc without the problems of a three-dimensional analysis. For the same level of depth of analysis in terms of computer time and core memory, one can model the interface between the disc and the centrum much more accurately in an axisymmetric than in a three-dimensional analysis. Now that the form of analysis has been obtained, the next step is to examine the centrum and the disc separately.

Two problems existed in modeling of the vertebral centrum: First, determining material properties for trabecular bone, cortical bone, and bony endplate, and secondly, accurately modeling the geometry of the bone. The modulus of elasticity and Poisson's ratio for human cortical and trabecular bone can be obtained from Belytschko (2). In addition, the modulus of elasticity of the vertebral centrum for both the human and rhesus monkey are known from Kazarian (8,9). However, the material constants for cortical or trabecular bone of the rhesus are not known. Kazarian (8) discusses the comparing of material characteristics between species. To obtain the material constants needed for the finite element model, several assumptions were made. First, it was assumed Poisson's ratio for human and rhesus bones were the same. Secondly, since centrum properties were available from both species, the ratio of the moduli of elasticity was used to estimate a modulus for the cortical and a modulus for the trabecular bone of the rhesus monkey. The ratio used to determine these constants was

$$\frac{E_{\text{human centrum}}}{E_{\text{rhesus centrum}}} = \frac{E_{\text{human cortical}}}{E_{\text{rhesus cortical}}} = \frac{E_{\text{human trabecular}}}{E_{\text{rhesus trabecular}}}$$

The final material properties were: $E_{\text{cortical}} = 6.207 \times 10^5 \text{ Kp/cm}^2$, $E_{\text{trabecular}} = 2.80 \times 10^3 \text{ Kp/cm}^2$ and both used $\nu = 0.25$. The bony endplate material properties are not clearly known. However, it is known to be harder than trabecular bone. As a result, the bony endplate was modeled with the same material properties as the cortical bone. The shape of the vertebral centrum also presented some problems. To solve this difficulty when the specimens were dissected, all measurements necessary to formulate the finite element model were taken. It was found that both the bony endplate and the cortical bone were extremely thin. As a result, a very fine mesh is needed to model both sections adequately. In addition, the fine mesh is needed to provide a good transition of the load from the trabecular bone to the disc. The disc will be modeled as a homogeneous body for several reasons. First, since the annulus is an orthotropic material and since it clearly displayed viscoelastic properties in the final creep test, to model it thoroughly would involve an orthotropic viscoelastic analysis with nine material constants. Obviously determining nine independent material constants is an awesome task. A second problem, in dividing up the disc, is how does one adequately model the fluid movement in the nucleus, annulus, and between the two materials? The problem here again is very difficult; fluid movement in a deforming body. In modeling the disk as a unit, one avoids many of the problems mentioned above. However, one does obtain information of the stress distributions and displacement profiles.

4.3 Coarse Mesh Analysis

The coarse mesh analysis served to provide excellent initial guesses to the fine mesh. However, from a finite element standpoint, the coarse mesh had several shortcomings.

The primary use of the coarse mesh was to provide information needed for the fine mesh. Since the coarse mesh had approximately one-fifth the number of variables of the fine mesh, one could run many more coarse mesh jobs in a day than fine mesh jobs. In addition, a clear relation existed between the spring constants (E_0, q_0) for the coarse model and the constants for the fine mesh (see fig. (4.3)). As a result, one could narrow in on material constant for the fine mesh quickly. A second advantage to the coarse mesh is that it provided an almost exact value for the dashpot constant, q_1 , for the fine mesh.

However, the coarse mesh did have several drawbacks. The most evident one is the high aspect ratios in both the cortical bone and bony endplate region (see fig. (4.3)). The second major problem to this mesh was the lack of transition from the trabecular to the disc region. The utility of the coarse mesh was in its ability to provide a good initial guess for the fine mesh.

4.4 Fine Mesh Analysis

The fine mesh analysis will be broken down into several sections. First a discussion of the formulation of the fine mesh, next each set of experimental data will be analyzed individually. First the healthy, then

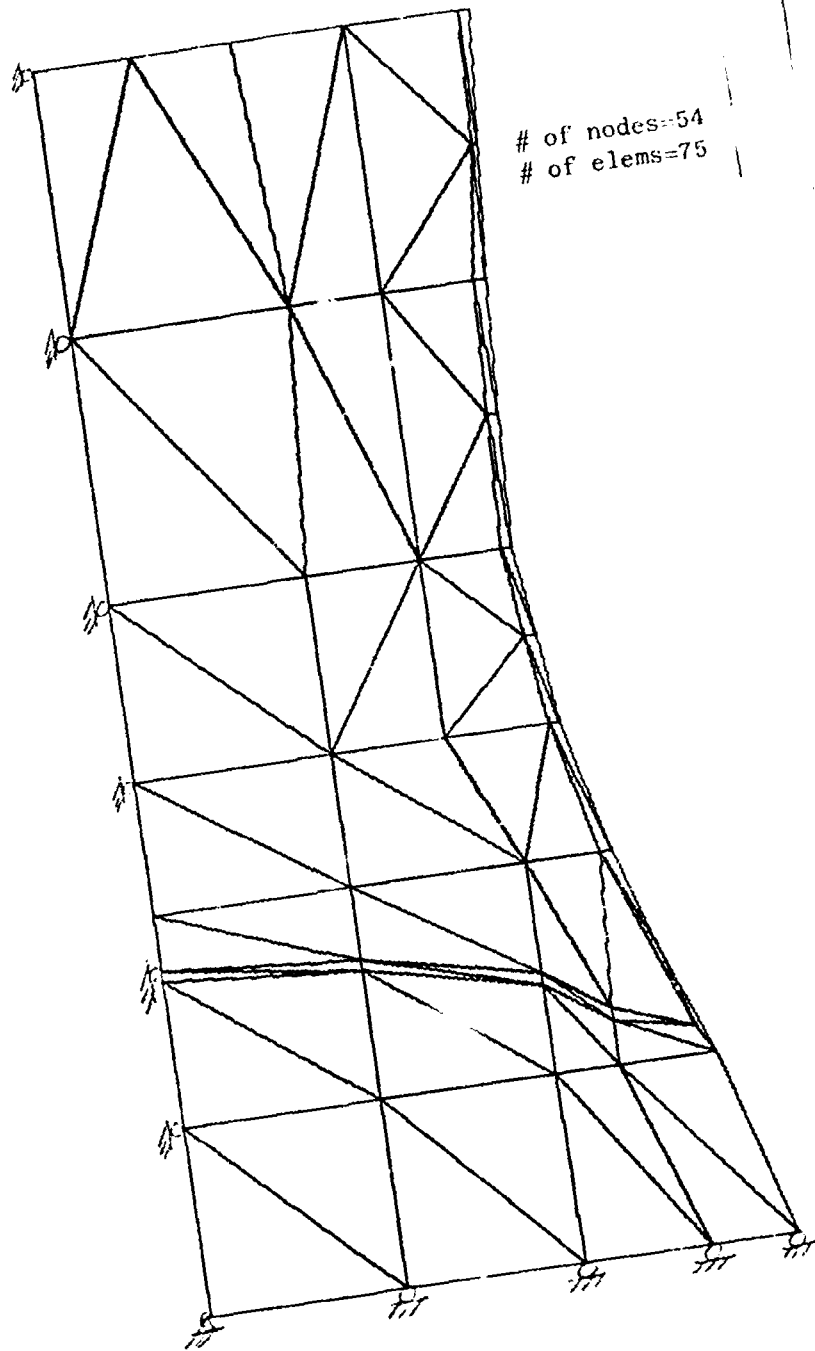


fig. 4.3 The coarse mesh had the advantage of quick turn around on the computer and providing an excellent first approximation for the fine mesh.

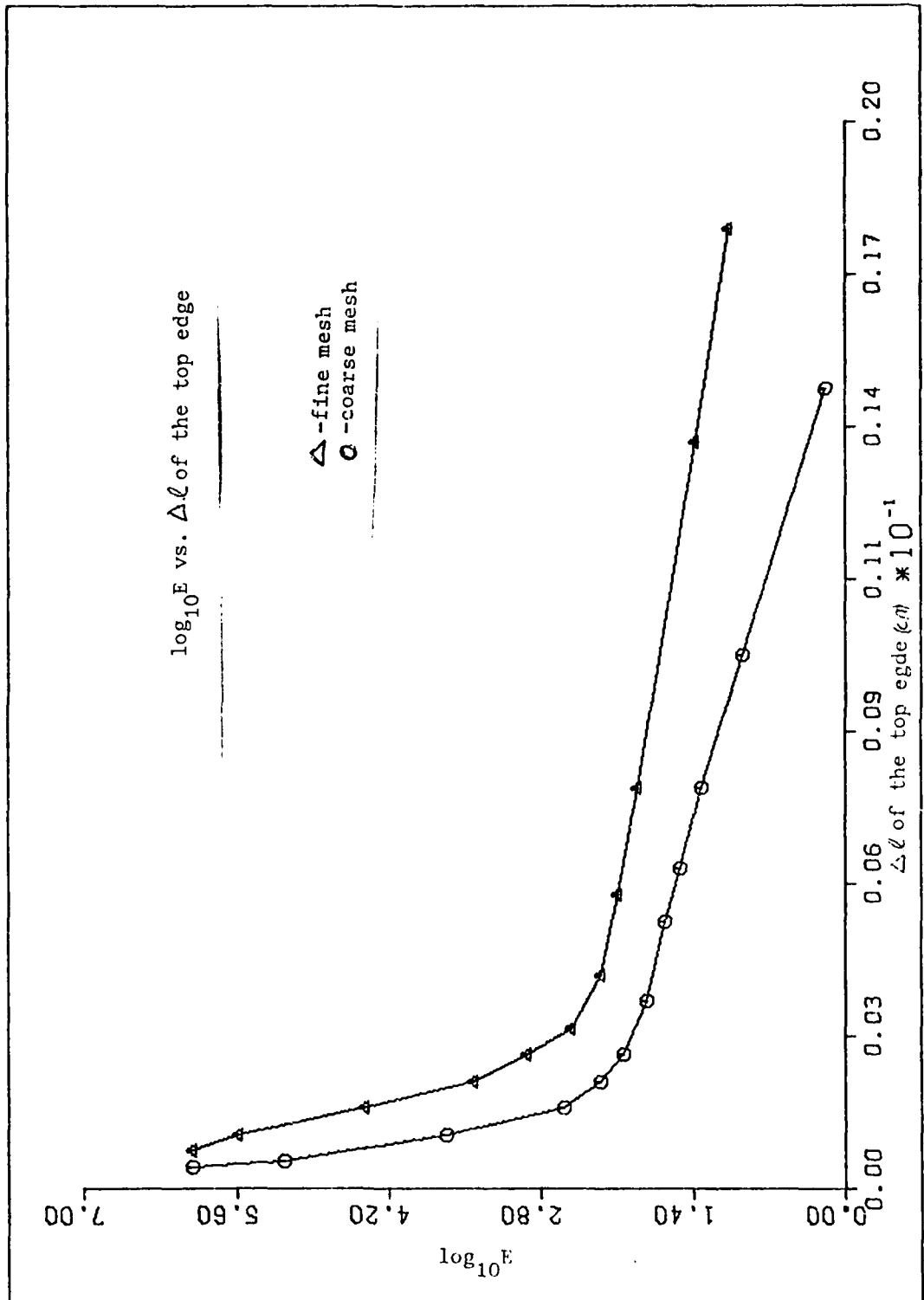


fig. 4.4 The above graph illustrates the relation between the spring constants, E_0 and q_1 , for the coarse to the fine mesh.

the fully herniated, and finally the osteo specimen will be studied. In the last section of this chapter, a comparison will be made between the three analyses.

The fine mesh model was obtained from two parameters: the need to show transition from one material to another and secondly using a progressively finer mesh to obtain a converged solution. The transition from one material to another was the primary reason for the fine mesh. The aspect ratio for all of the elements was reduced until the maximum was 3 to 1. At this point, the mesh was fine enough to obtain a converged solution also.

4.4.1 Analysis of the Healthy Specimen

The analysis of the healthy data can be examined at two levels: the ability of the model to match the displacement of the specimen and secondly, a discussion of stress flow in the specimen during the creep test.

The finite element model gave an excellent fit to the experimental results. For the fine mesh, the material constants which gave the best fit were $E_0 = 36.50 \text{ kp/cm}^2$, $q_0 = 16.21 \text{ kp/cm}^2$, $q_1 = 44060 \text{ kp/cm sec}$, and $\nu = 0.48$. The actual curve fit is shown in fig. 4.6. In addition, the radial displacement of the disc was very close to the experimental as can be seen in fig. 4.7. One can also see how the model deformed over time by examining figs. 4.8-4.10. Please note the displacements in the figures are multiplied by a factor of two to more clearly illustrate the deformations.

The finite element model also gave a good indication of the stress within the specimen. The graph of the θ , hoop stress versus radius in the centrum (fig. 4.11) shows that the cortical bone is acting like shell in compression restraining the trabecular bone. This becomes obvious if one looks at the geometry of the cortical bone. It is in the shape of an inwardly curved surface referred to as an anticlastic surface. Thus the radial tension and axial compression produce compression in the hoop direction. One can also note that the stress increases with time. Since the centrum has the same material properties in all three, analyses, it will not be covered in the discussion of the fully herniated or the osteo analysis. The stress data also gave numerous indications of the stress flow in the disc. The graph of the

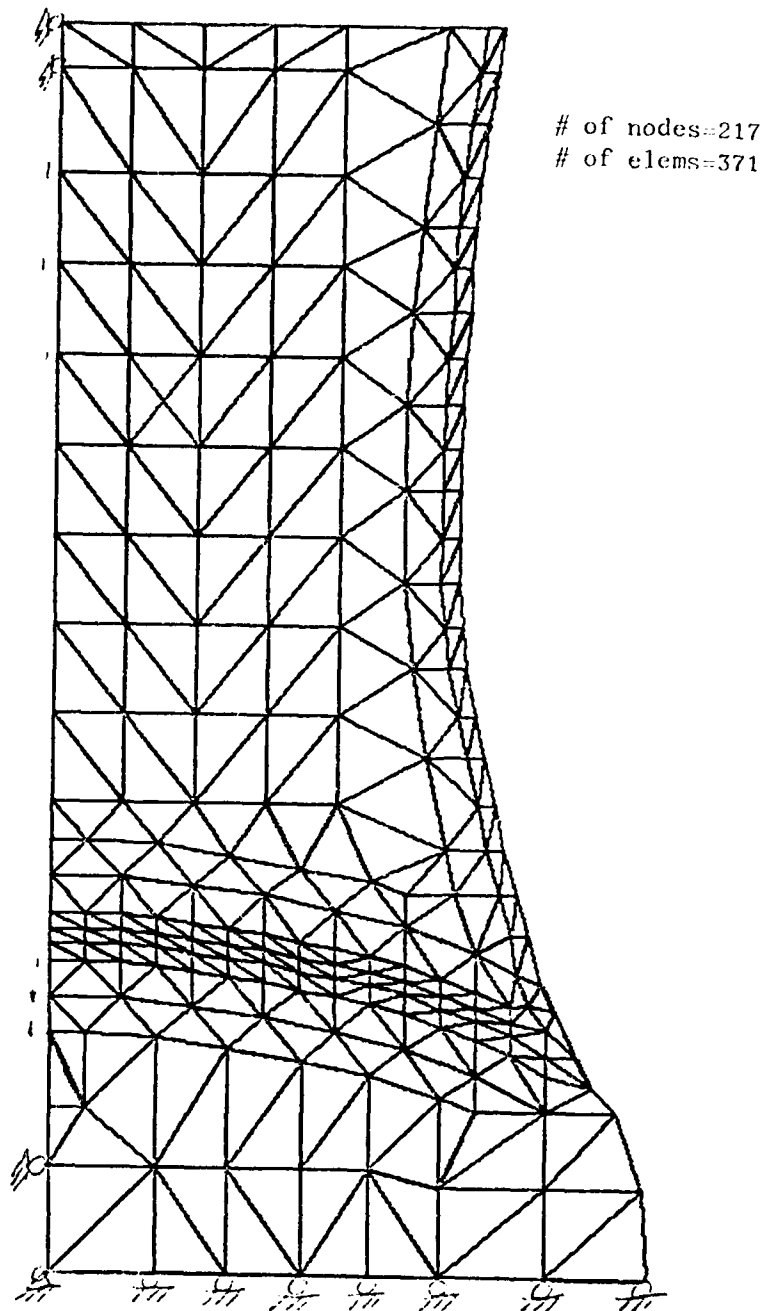


fig. 4.5 The size of the fine mesh was determined by using a progressively finer mesh.

radial stress versus radius (Fig. 4.12) clearly shows the bony endplate is compressing the disc except in the outer area of disc where the bony endplate does not cover the disc. In addition one can see that the stress level increases with time. The second graph in the disc region of the vertical stress versus radius (fig. 4.13) again shows the bony endplate is placing the disc in compression. One can again see the stress increases with time. The final pertains to the hoop stress in the disc (fig. 4.14) and shows an increase in the stress level with time. The graph also illustrates that the outer disc, which is not covered by the bony endplate, is in tension. This indicates the disc annulus region is resisting load as a shell structure. The outward radial curvature is indicative of a tension stress in the hoop direction arising from the axial compressive stress.

4.4.2 Analysis of the Fully Herniated Specimen

The analysis of the fully herniated test results will be covered in the same manner as the healthy. The displacements will be discussed first followed by the stress analysis.

The finite element model once again gave an excellent match to the experimental curves. The material constants which gave the best fit were $E_0 = 20.61 \text{ Kp/cm}^2$, $q_0 = 5.97 \text{ Kp/cm}^2$, $q_1 = 18500 \text{ Kp/cm sec}$, and $\nu = .480$. A graphical illustration of the fit is given in fig. 4.15. One can also see deformation of the model in figs. 4.16 - 4.17.

The stress profiles also give a good indication of the stress

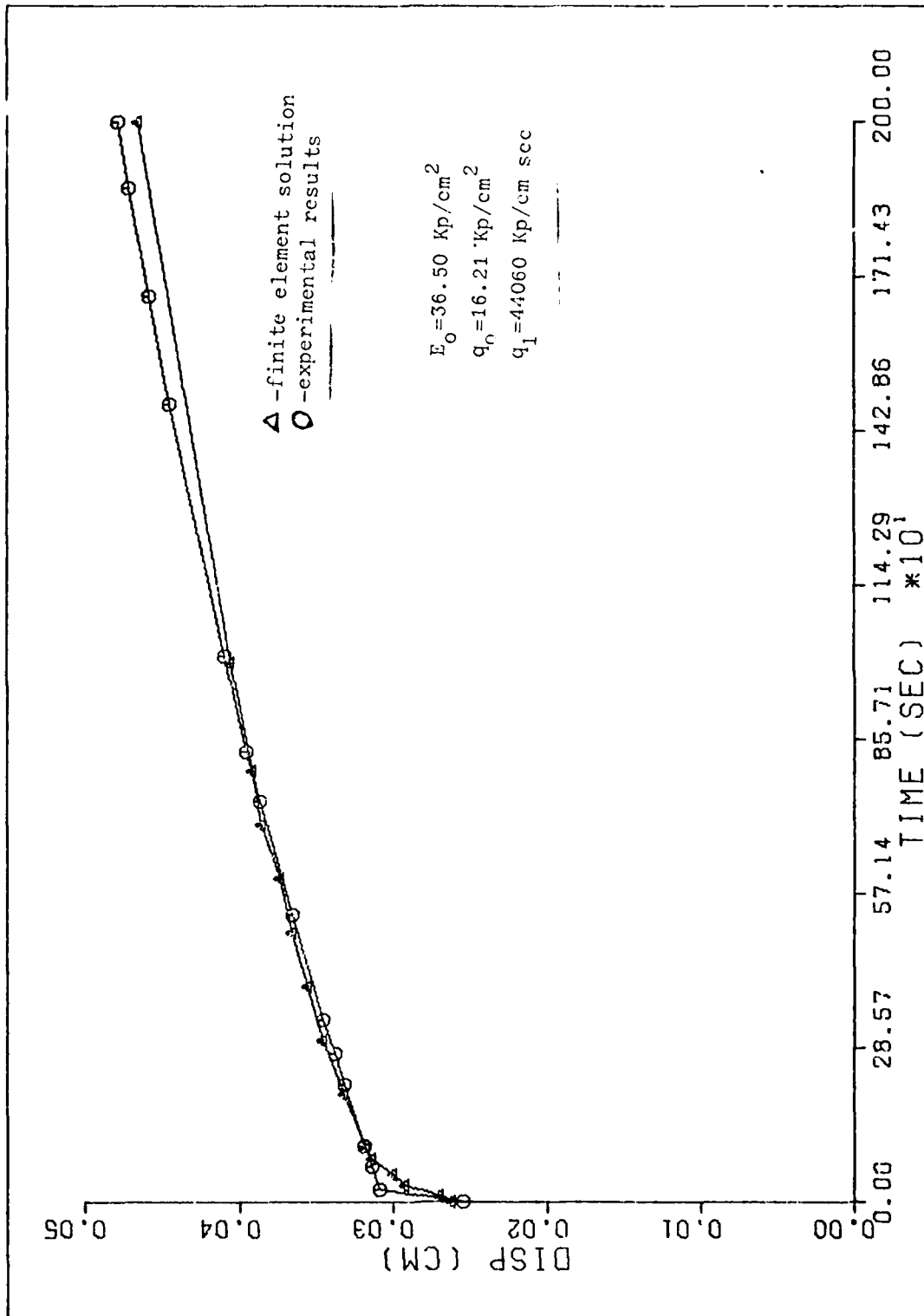


fig. 4.6 Finite element solution for vertical displacement of the healthy specimen

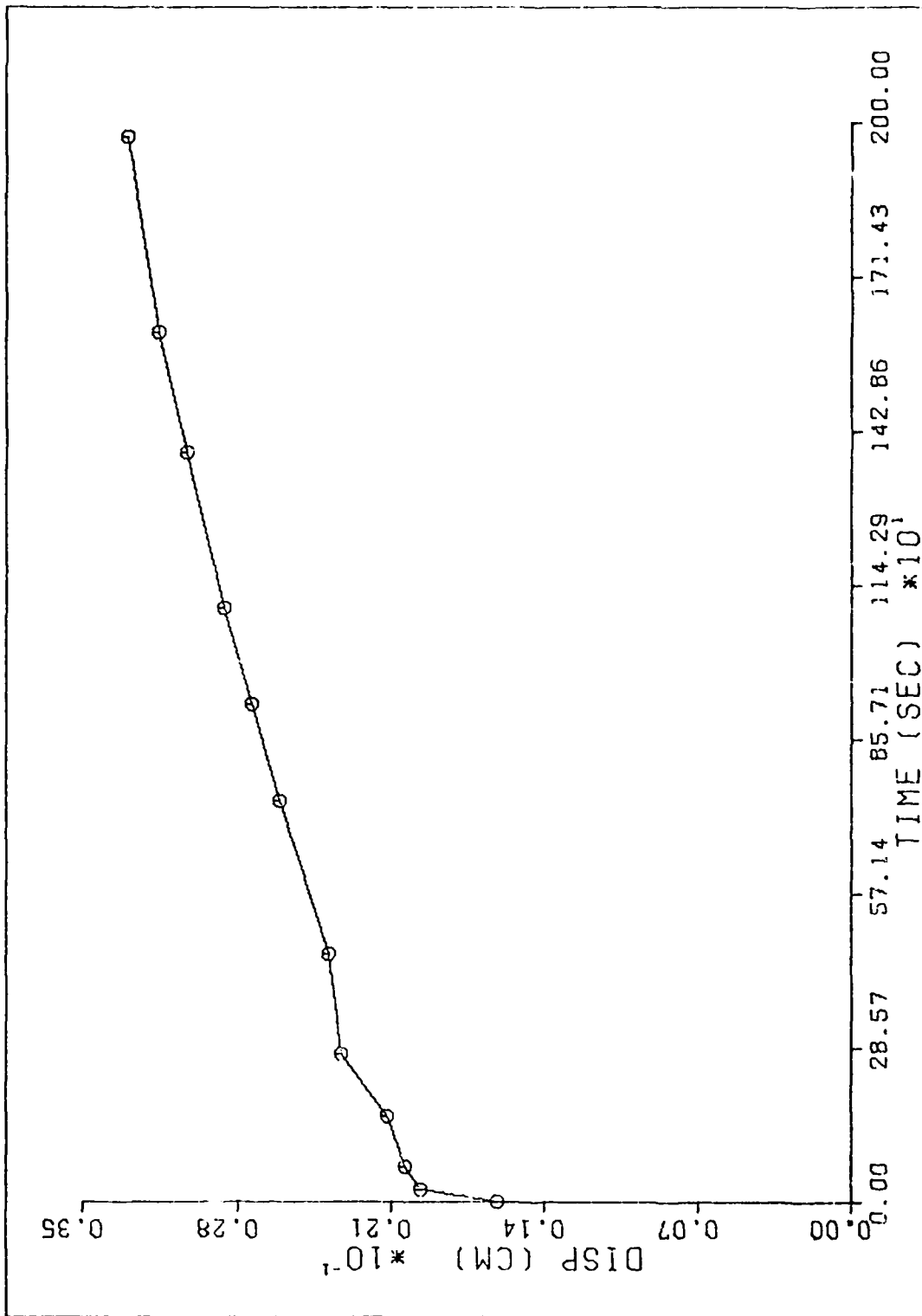


fig 4.7 Finite element solution of radial displacement in the disc of the healthy specimen.

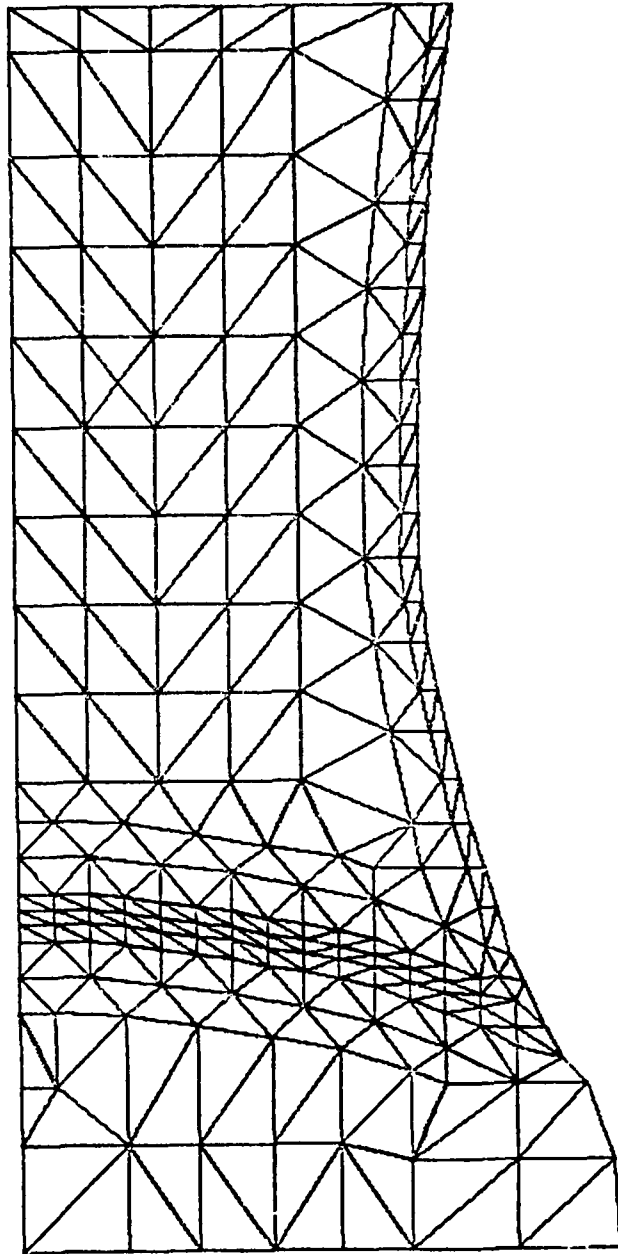


fig. 4.8 Fine finite model of healthy specimen.

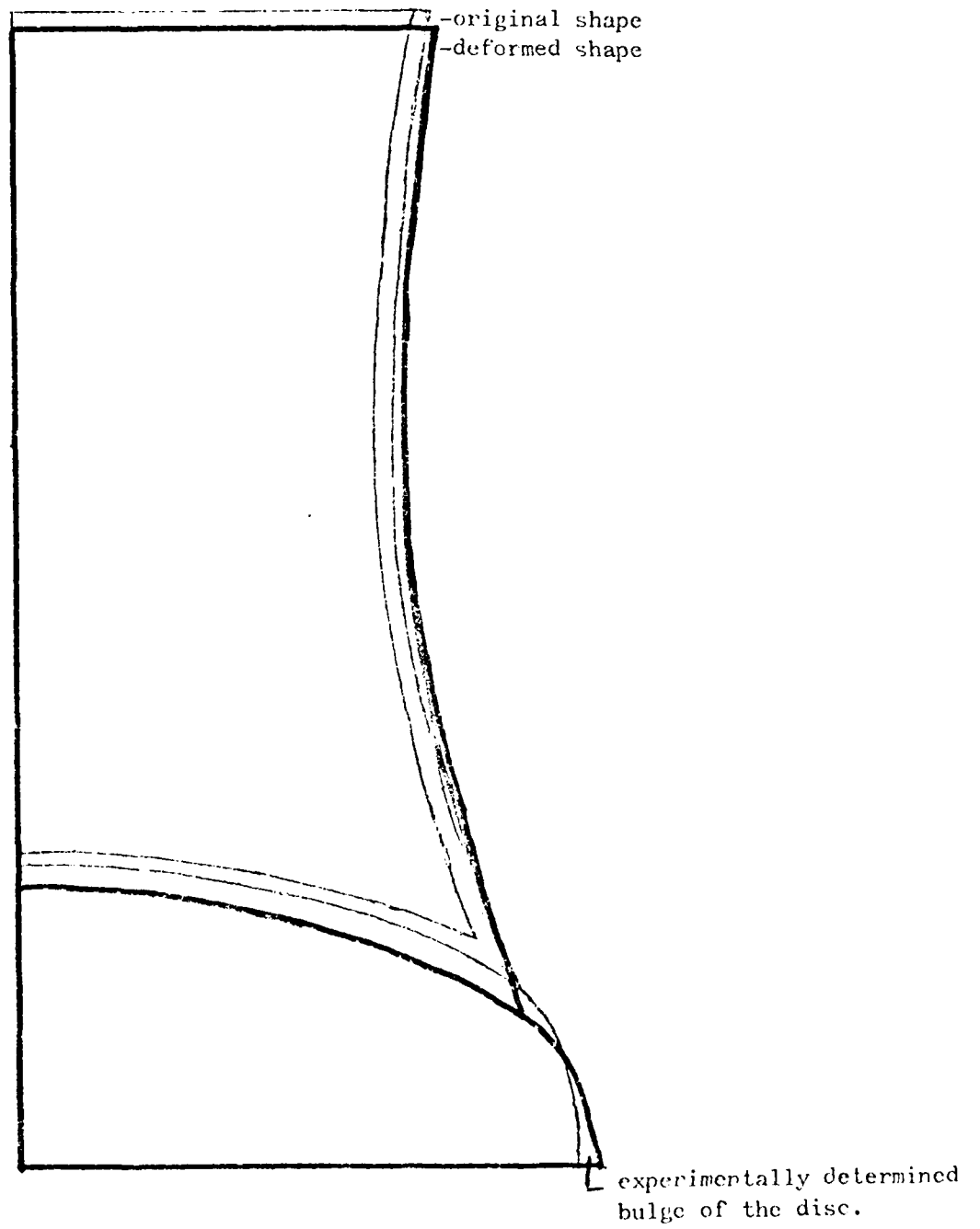


fig. 4.9 Displacement of healthy specimen at $t=0^+$.

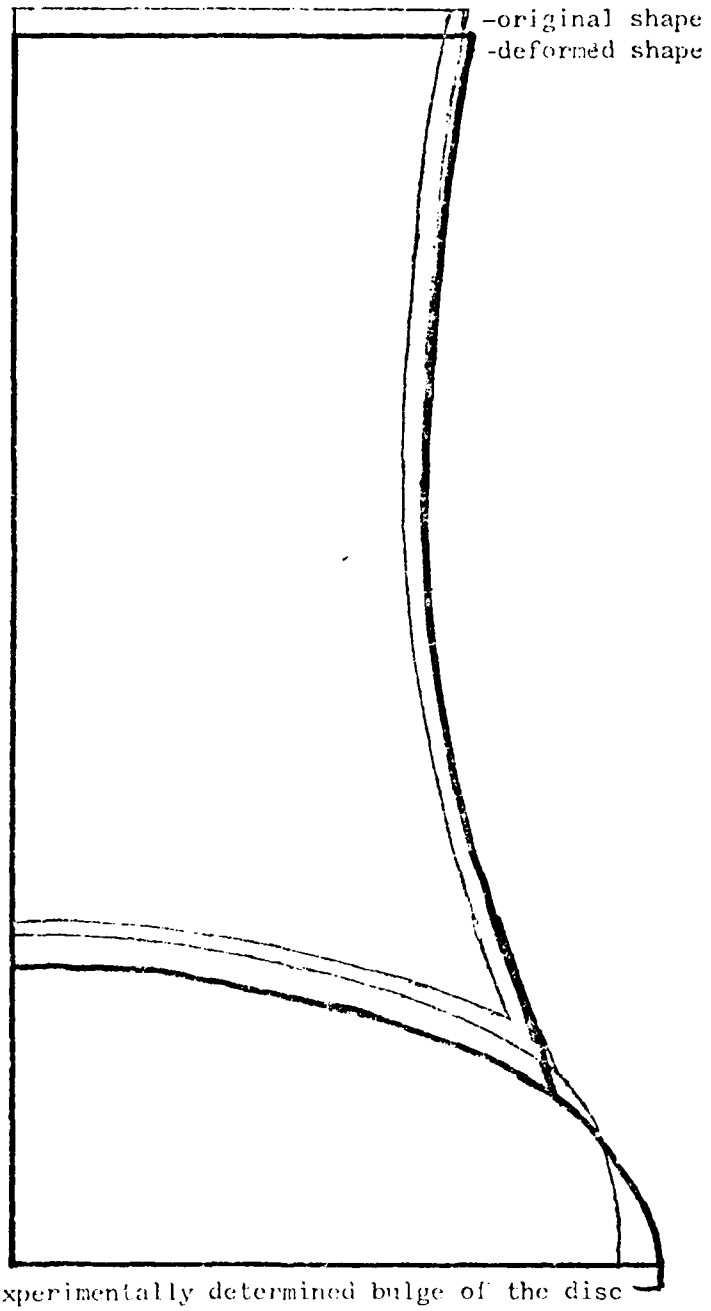


fig. 4.10 Displacement of the healthy specimen at $t=1500\text{sec.}$

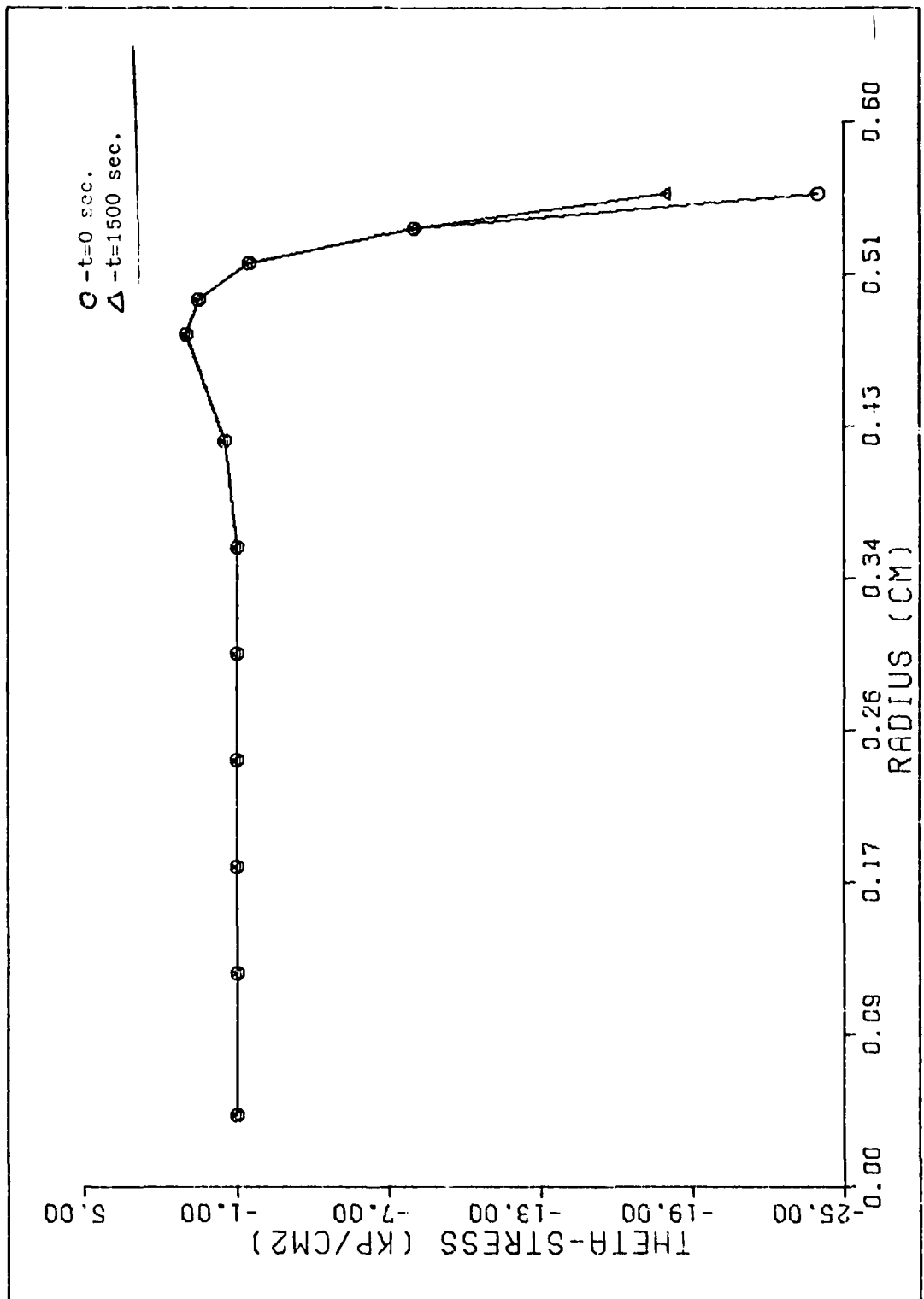


Fig. 4.11 Hoop stress versus radius in the centrum.

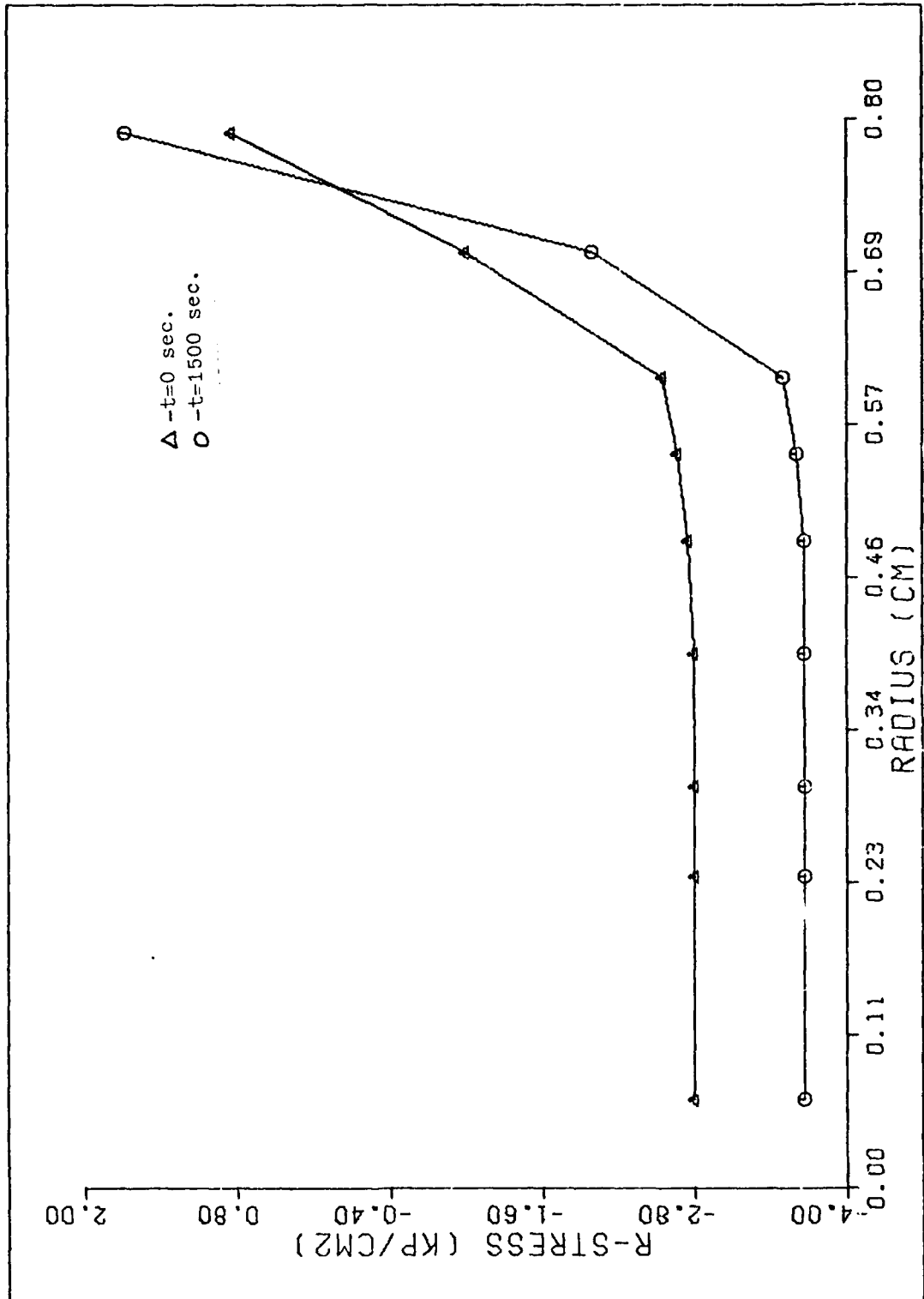


fig. 4.12 Radial stress versus radius in the disc of the healthy specimen.

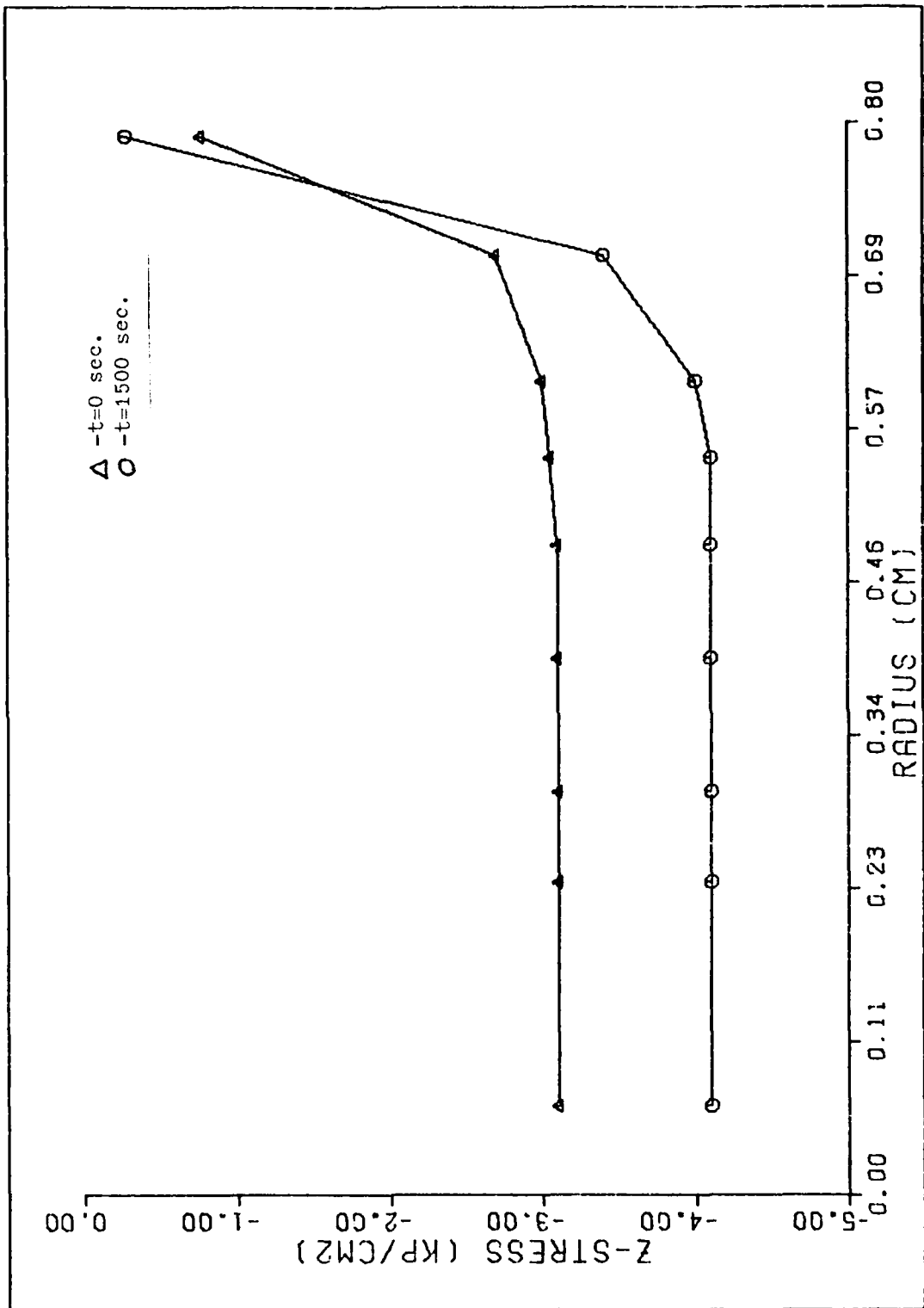


fig. 4.13 Vertical stress versus radius in the disc of the healthy specimen.

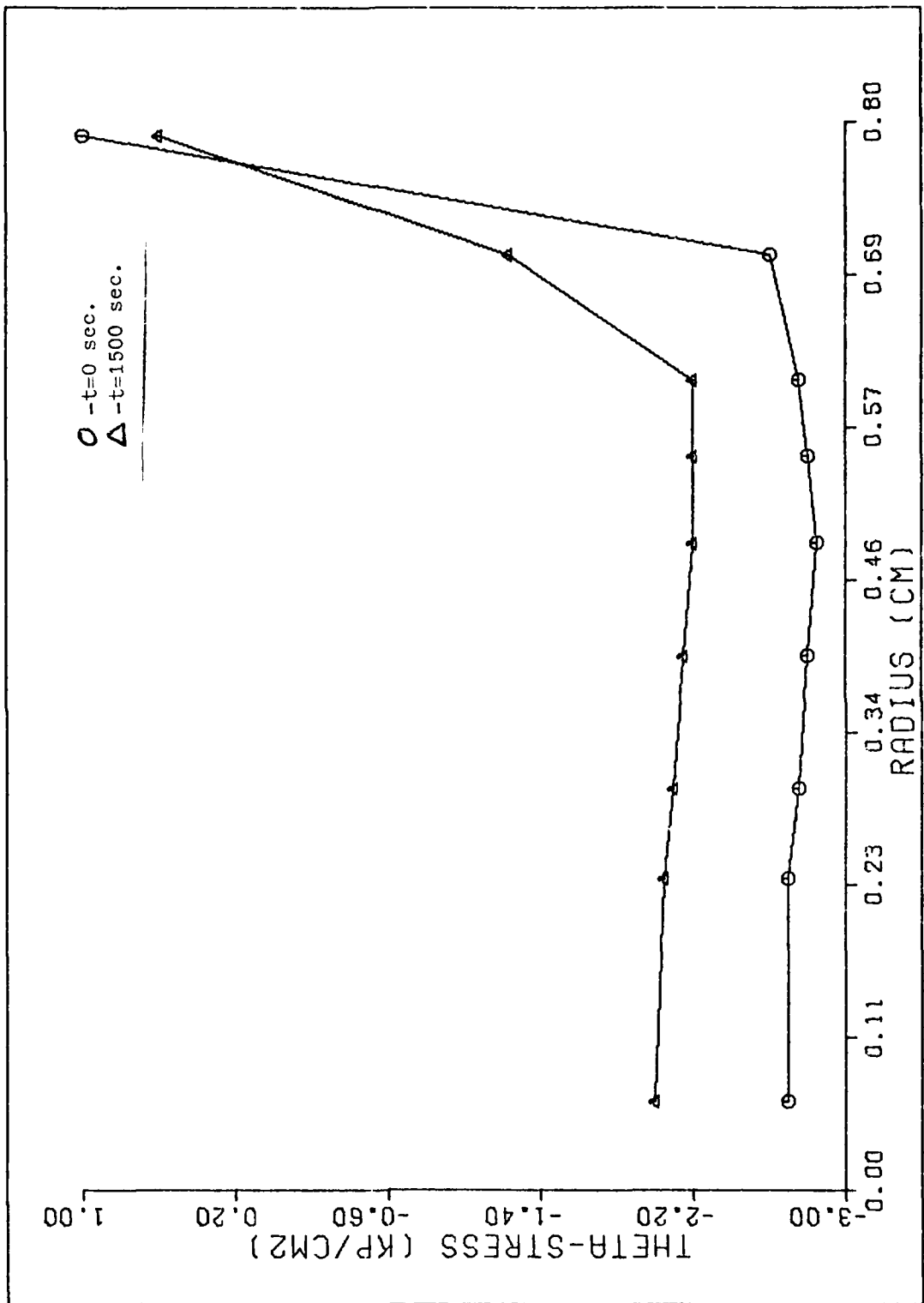


fig. 4.14 Hoop stress versus radius in the disc of the healthy specimen.

redistribution with time. The first graph in fig. 4.18 of the radius stress in the disc shows the stress decreasing as the radius increases. In addition, one can see the total radial stress increases with time. The second graph in the disk region of the vertical stress versus radius (fig. 4.19) again shows the bony endplate is placing the disc in compression. However, in this curve the entire disc is in compression. One can again see the stress increases with time. The final curve pertains to the hoop stress in the disc (fig. 4.17) and shows an increase in stress level with time. This hoop stress profile is again showing that the nature of restraint by the disc as a shell structural element.

4.4.3 Analysis of the Osteo Specimen

Before discussing the analytical results, a brief description of the diseased state of the osteo specimen will be helpful. The osteo specimen was diagnosed by a veterinarian to have osteochondritis. From the X-ray, one could see the bony endplate of the upper centrum extended well into the nucleus to point at which almost no nucleus was present in the disc. The same analytical model was used to study this specimen as the previous two data sets. In the analysis of the osteo experimental data, the same type of information was obtained as in the two previous models. The displacement curves will be studied first, followed by the stress analysis.

The finite element model once again gave a very close correlation to the experimental data. The best curve fit were with material constants of $E_0 = 56.25 \text{ Kp/cm}^2$ $q_0 = 9.218 \text{ Kp/cm}^2$ $q_1 =$

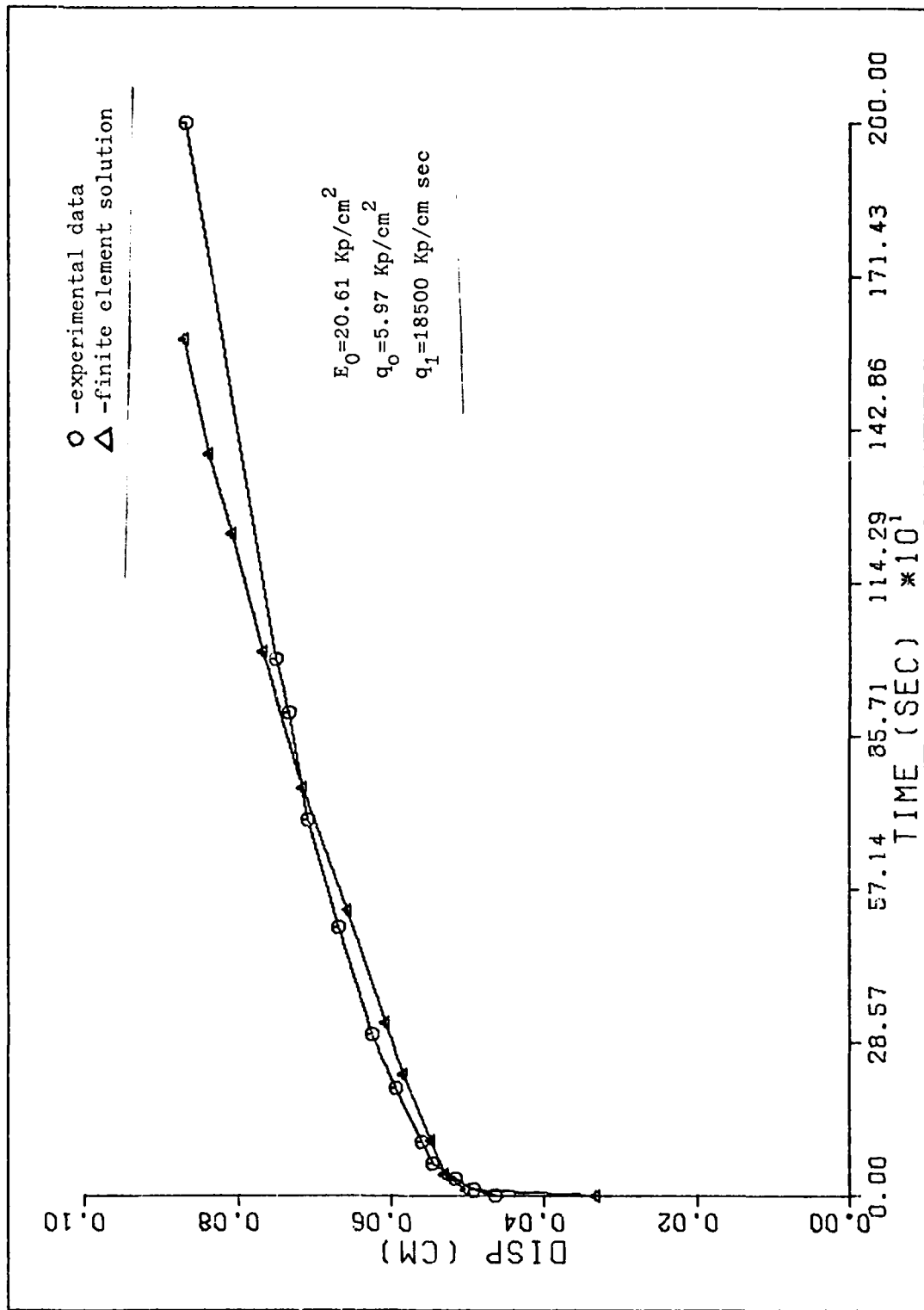


fig. 4.15 Finite element solution of fully herniated specimen.

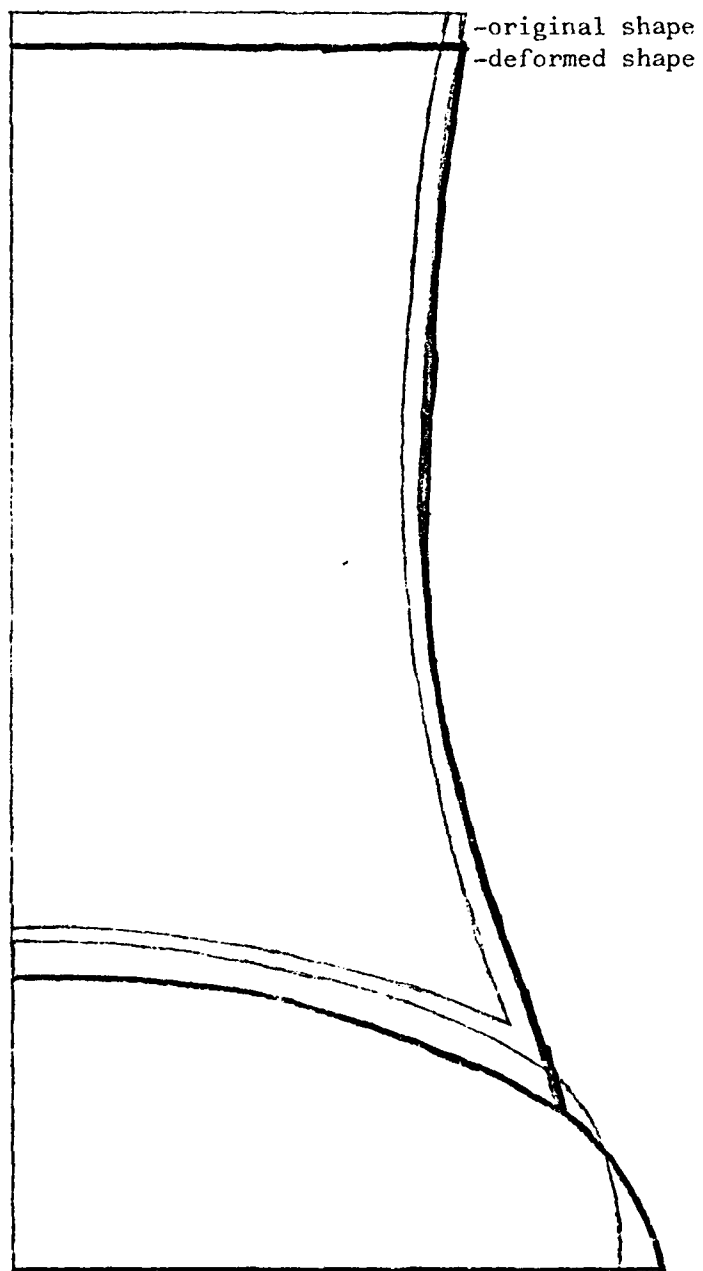


fig. 4.16 Displacement of fully herniated specimen at $t=0^+$

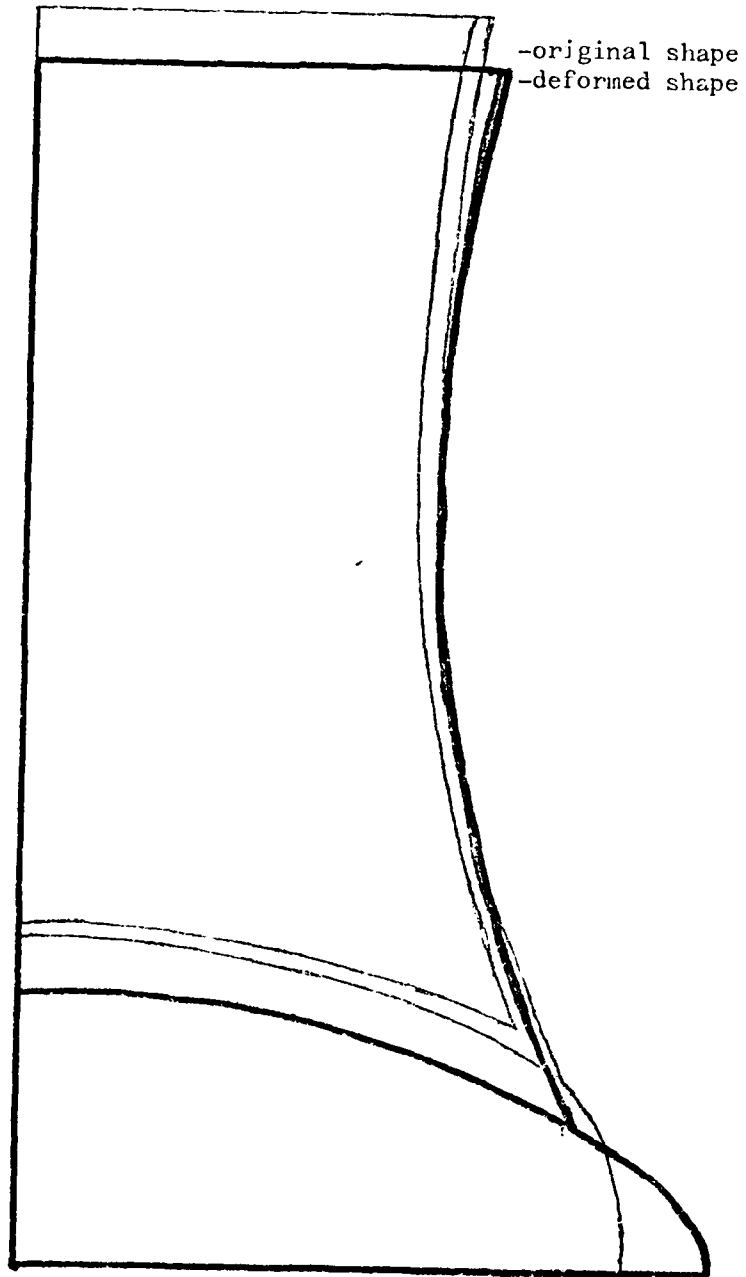


fig. 4.17 Displacement of the fully herniated specimen at $t=1500$ sec.

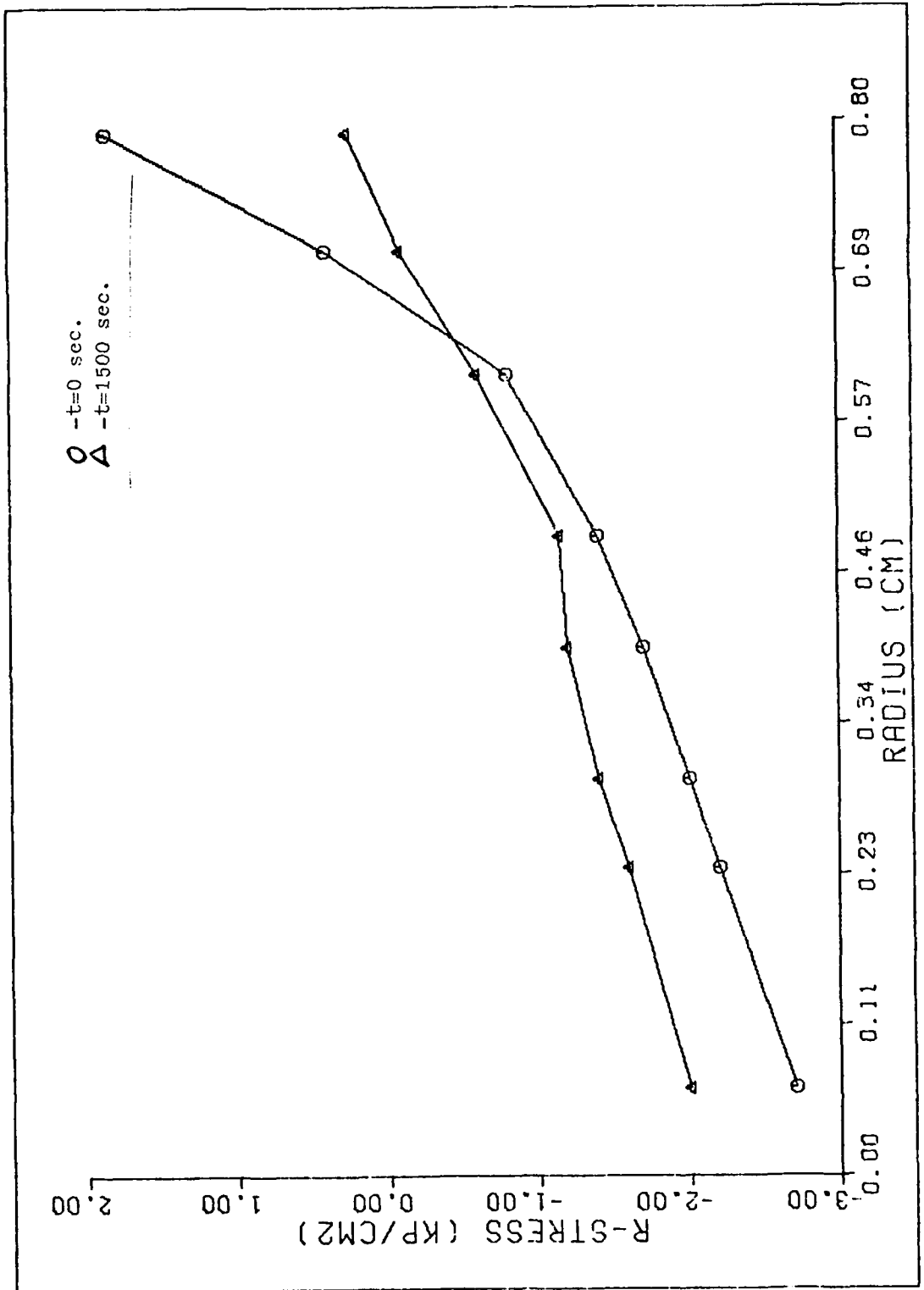


fig. 4.18 Radial stress versus radius in the disc of the fully herniated specimen.

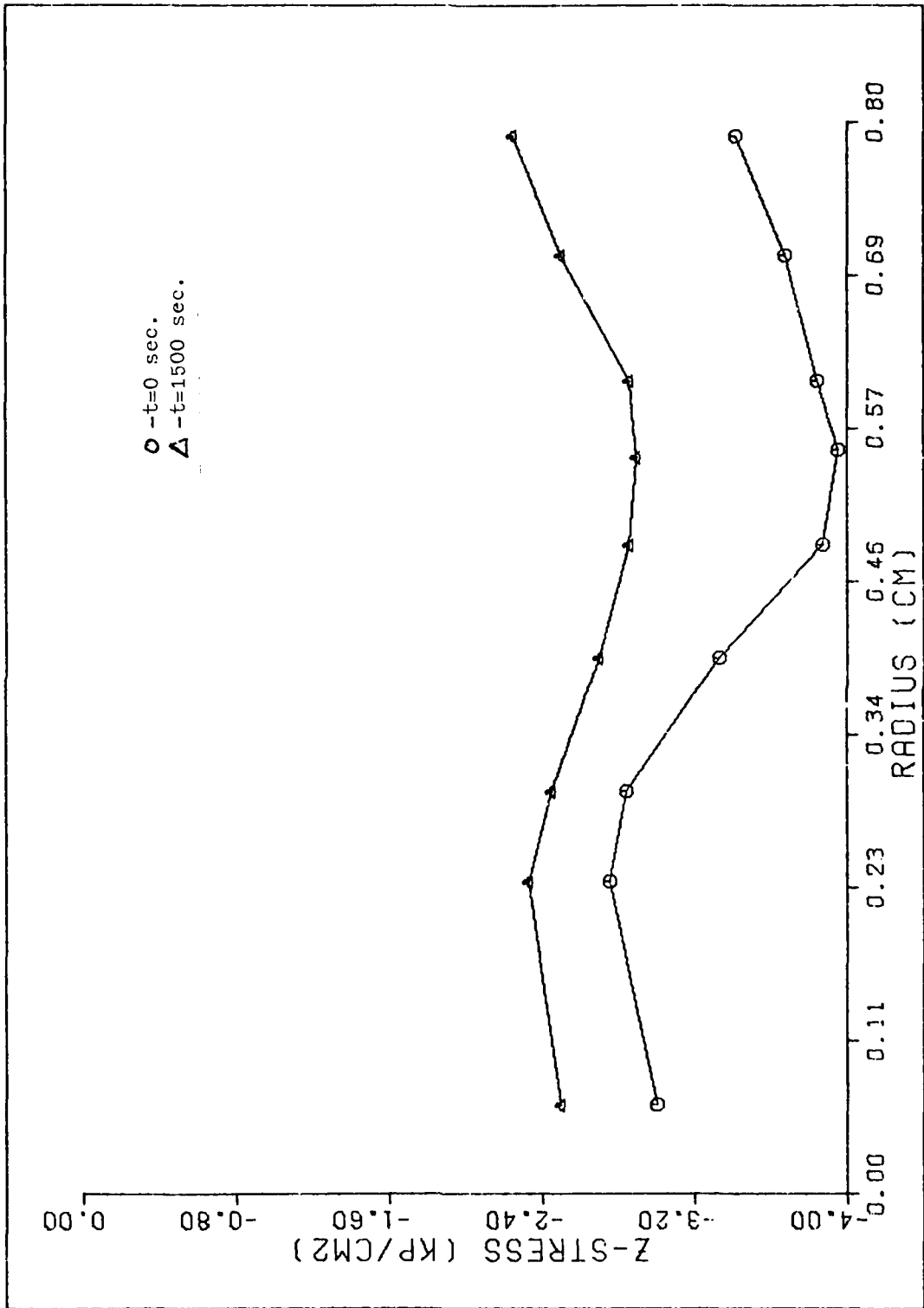


fig. 4.19 Vertical stress versus radius in the disc of the fully herniated specimen.

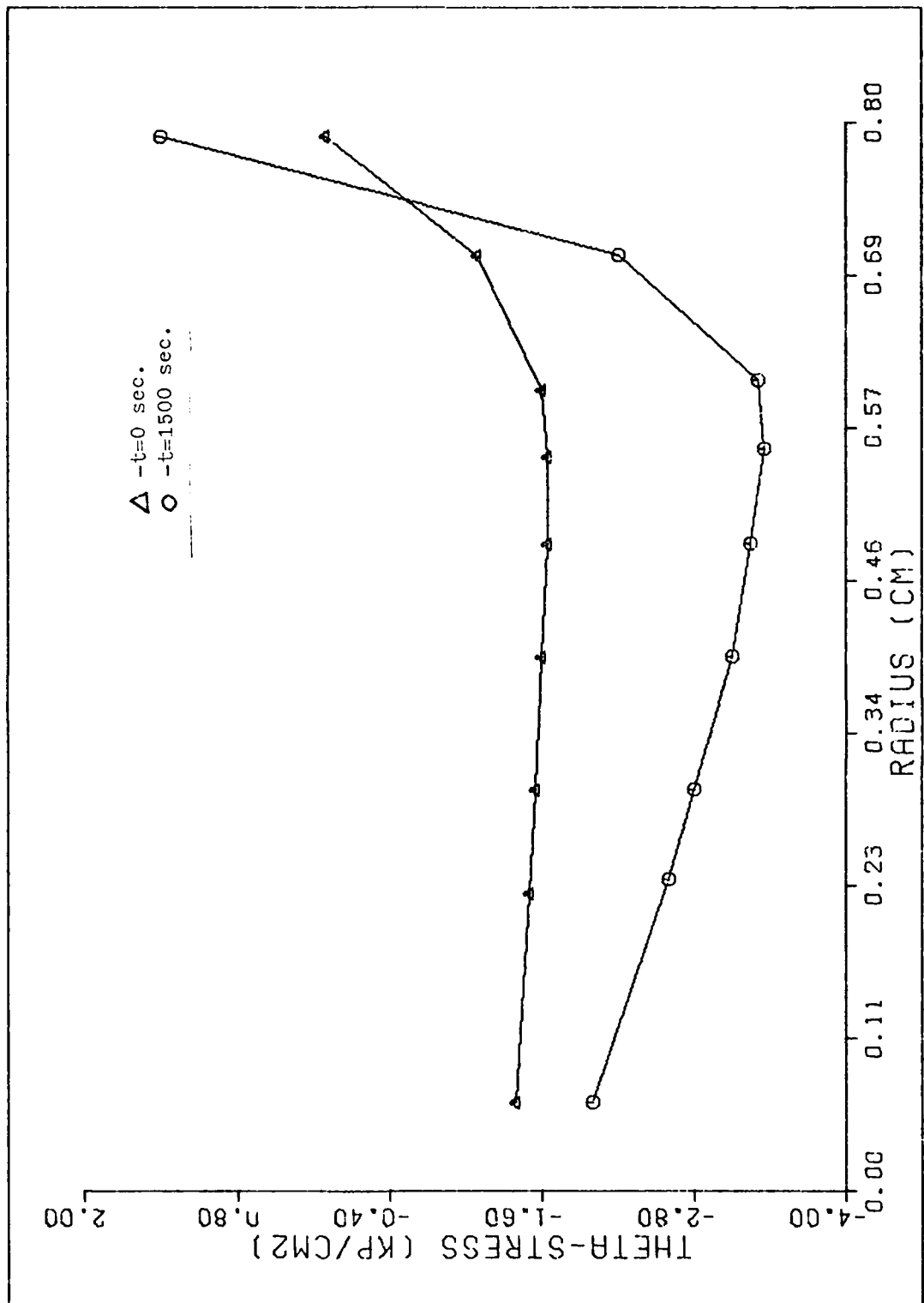


fig. 4.20 Hoop stress versus radius in the disc of the fully herniated specimen.

27030 Kp/cm sec and $= .480$. The finite element solution is shown in fig. 4.21. Once again deformed plots were made of the specimen and are shown in fig. 4.22-4.23.

The stress profiles were made to show the stress redistribution. The radial stress (fig. 4.24) shows the disc compression in all areas except the region which is not covered by the bony endplates. The stress in the z direction (fig. 4.25) also shows the disc in compression. The stress curve of the hoop stress shows to the disc in compression except in the outer region of the disc. Once again, all three stresses increase with time. The z-stress, shown in fig. 4.25, shows compression throughout the disc. In addition, one can see the stress again increasing with time. The graphs of the hoop stress, fig. 4.26 shows the disc in compression in all areas except the outermost area of the disc where it is not covered by the endplate. Again, this is an indication of the shell-like restraint of the disc's edge upon the inner nucleus as discussed previously.

4.4.4 Comparison of Analytical Results

The comparison of the analytical results will be done in two phases: first the healthy analysis will be compared to that of the fully herniated and second the healthy analysis will be compared to that of the osteo.

The comparison of the healthy analysis to the fully herniated indicates the influence of the nucleus pulposus on the viscoelastic material property. The elastic constant, E_0 , is approximately double for the healthy, $E_0 = 36.5 \text{ Kp/cm}^2$ compared to the fully herniated

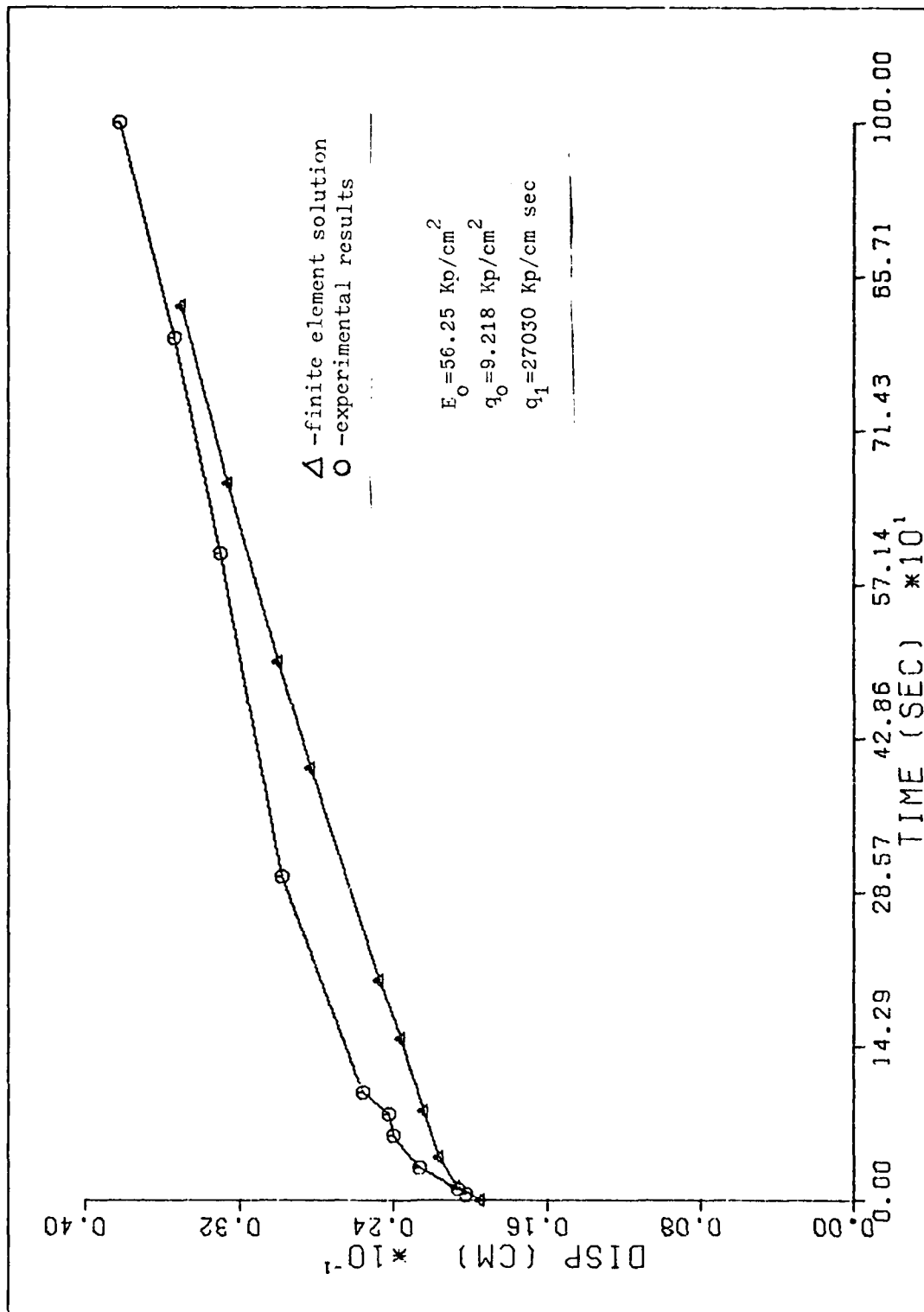


fig. 4.21 Finite element solution of Osteo specimen.

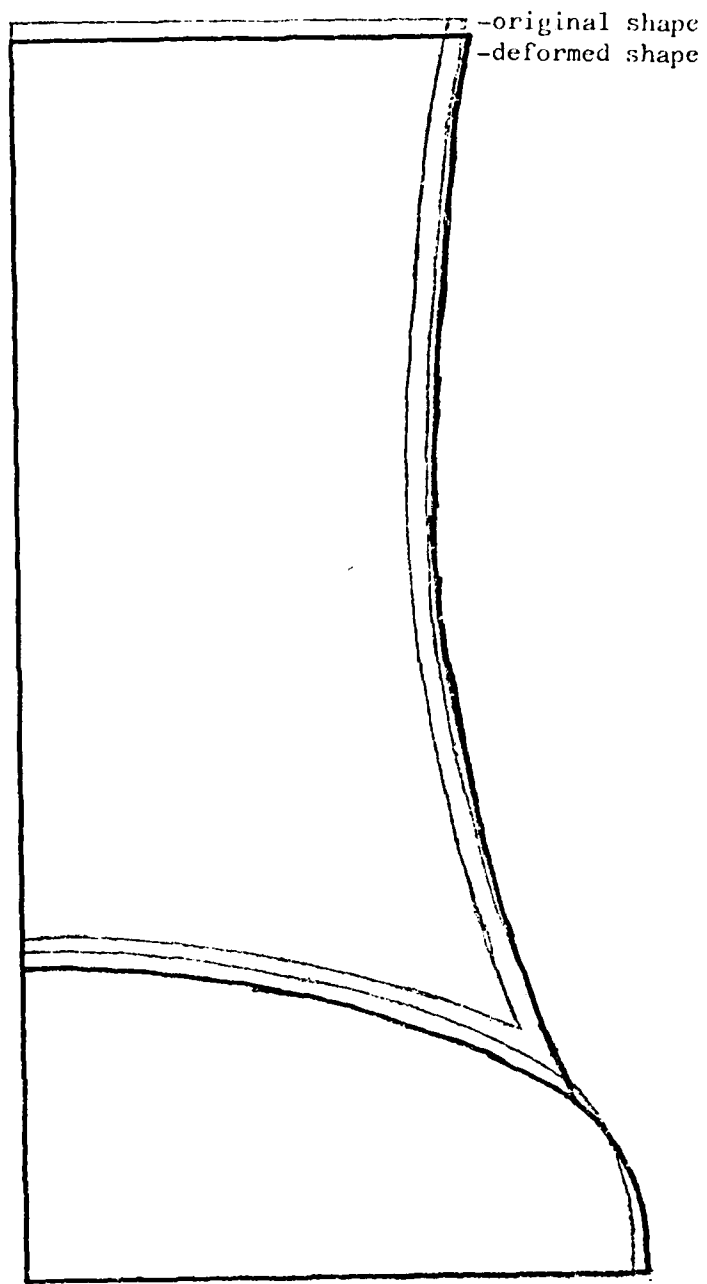


fig. 4.22 Displacement of the Osteo specimen at $t=0^+$.

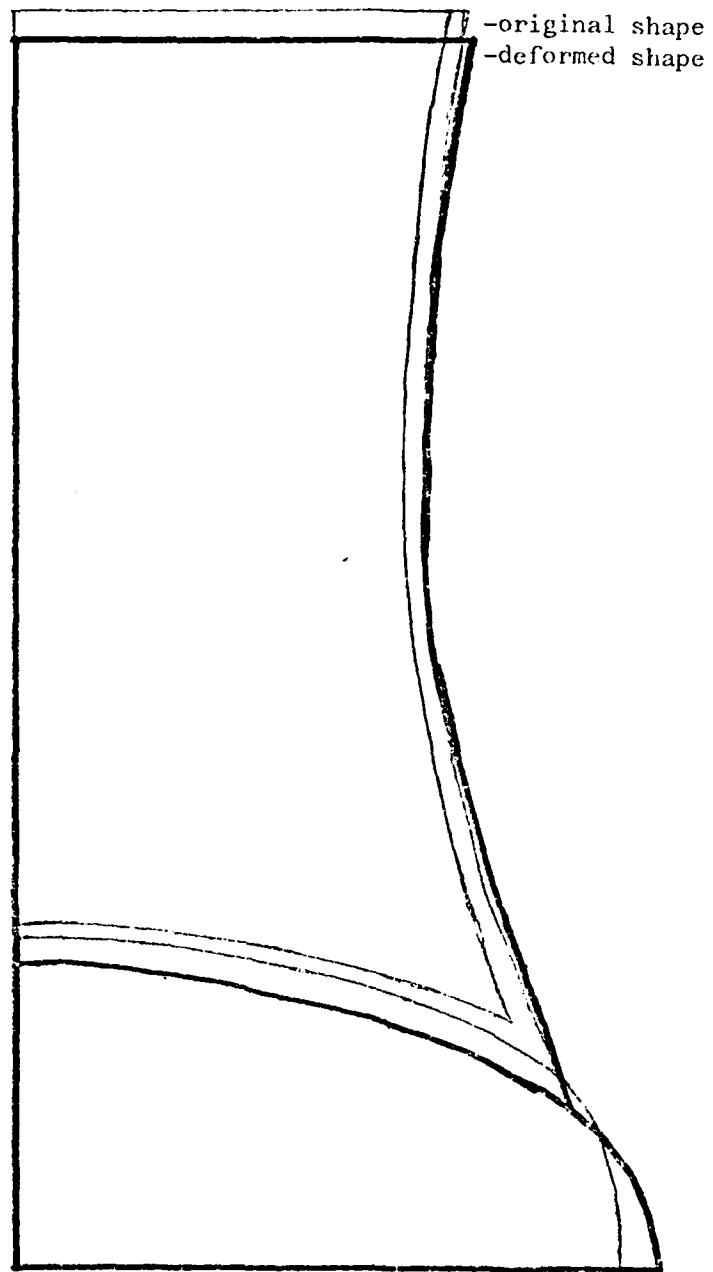


fig. 4.23 Displacement of the Osteo specimen at $t=830$ sec.

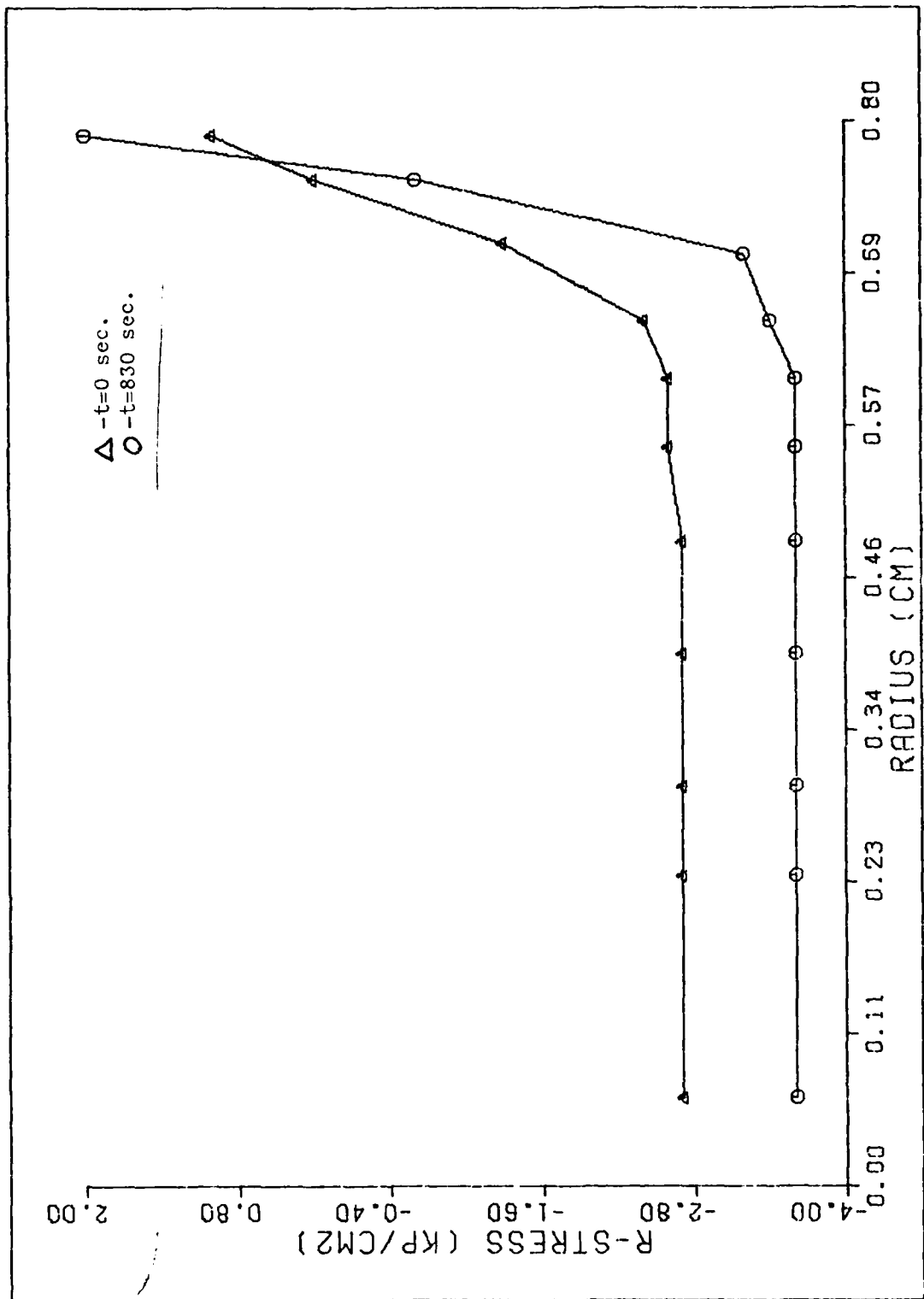


fig. 4.24 Radial stress versus radius in the disc of the Osteo specimen.

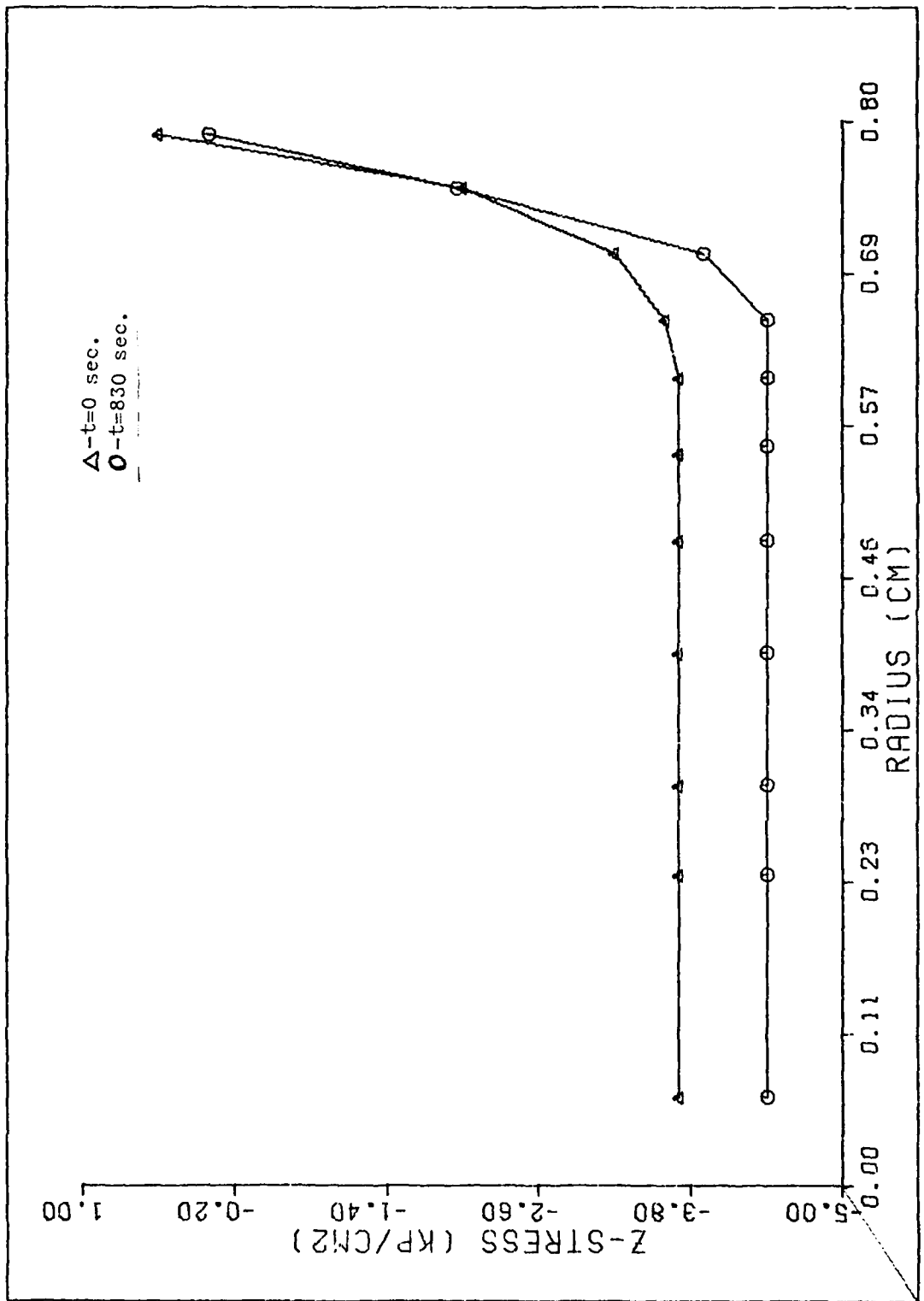


fig. 4.25 Vertical stress versus radius in the disc of the Osteo specimen.

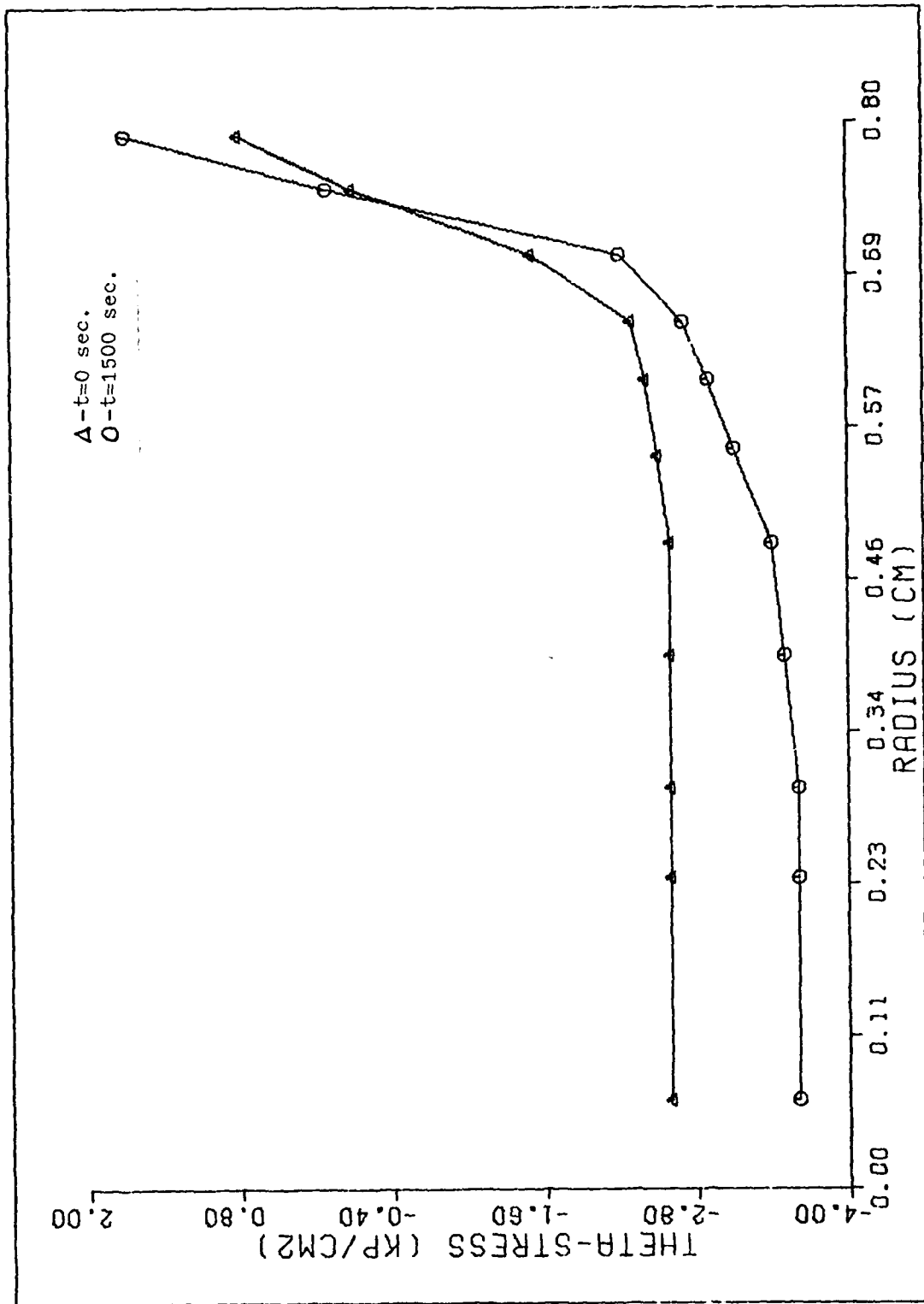


fig. 4.26 Hoop stress versus radius in the disc of the Osteo specimen.

$E_0 = 20.6 \text{ Kp/cm}^2$. In addition, the Kelvin solid unit for the herniated not only gave a larger final displacement but the creep rate was much faster than the healthy. The stress curves also show that the increase in all stress levels was greater for the herniated than the healthy. From the comparison of the material constants and the stress levels, one can conclude that the disc not only acts as a structural member but also assist in redistributing the stress in the specimen over time.

The correlation between the osteo specimen and the healthy was closer than that of the herniated to the healthy. However, several differences did exist. The osteo specimen had a significantly elastic spring constant than the healthy: $E_0 = 36.5 \text{ Kp/cm}$ for the healthy and $E_0 = 56 \text{ Kp/cm}^2$ for the osteo. Yet the Kelvin solid unit in the osteo crept at a higher rate than the healthy. In comparing the stress analysis between the two data sets, very little difference is present at either the initial time or for large time values.

Chapter 5

Conclusions

In the final examination of this problem, one can make statements in several areas: the experimental procedure, viscoelasticity of the annulus fibrosis and the nucleus pulposus, an example of the self-sealing mechanism, and lastly the advantages of an axisymmetric analysis.

The experimental results yielded several important conclusions. By cupping of the specimen before loading, it was possible to achieve a purely compressive displacement and avoid pitch and torsion as encountered by other experimenters. The load was also evenly distributed across the top edge of the specimen. By keeping the specimens in a high humidity environment throughout the experimentation, it was possible to make several load cycles on each specimen in varying states of herniation without inducing changes in material properties due to water loss.

The viscoelastic response was present in all specimens. Yet, Kazarian (11) has found in certain cases that the loss of the nucleus pulposus results in loss of the viscoelastic response. A possible explanation for this would be that a latent period exist when the disc continues to behave in a viscoelastic manner after loss of the nucleus. As a result, one should not discount the importance of the disc in the viscoelastic response. The healthy disc also showed a smaller displacement for the same stress level than the herniated. A physical interpretation of this would be the healthy specimen is stiffer and thus

undergoes a smaller displacement for the same load.

In the first attempt at herniation, the creep curve was almost identical to the healthy. A possible explanation of this was found in White's text (18). He stated that the annulus has a self-sealing mechanism to prevent loss of the nucleus. This study is an excellent example of the mechanism. In addition, one can now conclude that to test only the annulus one must negate the nucleus as a structural component.

Finally, the advantages of an axisymmetric analysis give one a feel for the stress flow within the specimen. The stress in the cortical bone resisting the flow of the trabecular bone under compression shows the cortical bone is behaving similar to a doubly curved anticlastic hyperboloid of revolution shell restraining the trabecular bone. Furthermore, it appears that due to the constraint imposed by the bony endplate the outer region of the disc is acting similar to a doubly curved synclastic shell of revolution characterized by the tension in the hoop direction.

BIBLIOGRAPHY

1. Anderson, Gunnar B. J. and Schultz, Albert B. "Effects of Fluid Injection on Mechanical Properties of Intervertebral Discs," Journal of Biomechanics, Vol 12: pp. 453-458, 1979.
2. Belytschko, T., Kulak, R. K., Schultz, A. B., and Galante, J. O. "Finite Element Analysis of an Intervertebral Disc," Journal of Biomechanics, Vol 7: pp. 277-285, 1979.
3. Burns, M. L. and Kaleps, I. "Analysis of Load-Deflection Behavior of Intervertebral Discs Under Axial Compression Using Exact Parametric Solutions of Kelvin-Solid Models," Journal of Biomechanics, Vol 13: pp. 954-964, 1980.
4. Függe, Wilhelm. "Viscoelasticity," Waltham, Mass: Blaisdell Publishing Company, 1967.
5. Fung, Y. C. "Biomechanics (its scope, history and some problems of continuum mechanics in physiology)," Appl. Mech. Rev., Vol 21: pp. 1-20, 1960.
6. Hinrichsen, Ronald L. "A Viscoelastic Finite Element Model of the Human Intervertebral Joint," M.S. Thesis, Air Force Institute of Technology, Dec. 1980 (AFIT/GAE/AA/800-11).
7. Hirsch, Carl. "The reaction of Intervertebral Disc to Compressive Forces," The Journal of Bone and Joint Surgery, Vol 37A: No. 6, p. 1188, Dec. 1955.
8. Kazarian, Leon E. and von Gierke, Henning. "The Validation of Biodynamic Models," AMRL-TR-78-105, Wright-Patterson AFB, Aerospace Medical Research Laboratory, November, 1978 (AD A-080345).
9. Kazarian, Leon E. and Graves, George. "Compressive Strength Characteristics of the Primate (Macaca mulatta) Vertebral Centrum," AMRL-TR-79-8, Wright-Patterson AFB, Aerospace Medical Research Laboratory, May 1979.
10. Kazarian, Leon E. and Graves, George A. Jr. "Compressive Strength Characteristics of the Human Vertebral Centrum," Spine, Vol 2: No. 1, p. 1, March 1977.
11. Kazarian, Leon E. and Kaleps, Ints. "Mechanical and Physical Properties of the Human Intervertebral Joint," AMRL-TR-79-3, Wright-Patterson AFB, Aerospace Medical Research Laboratory, 1979.
12. Kulak, M. and Galante, J. O. "Nonlinear Behavior of the Human Intervertebral Disc Under Axial Load," Journal of Biomechanics, Vol 9: pp. 377-386, 1976.
13. Lin, H. S., Liu, Y. K., Ray, Gautom, and N. Kravesh, P. "System Identification for Material Properties of the Intervertebral Joint," Journal of Biomechanics, Vol 11, pp. 1-14, 1978.

14. Lin, H. S. and Liu, Y. K. "Mechanical Response of the Lumbar Intervertebral Joint Under Physiological (Complex) Loading," The Journal of Bone and Joint Surgery, p. 41, Vol 60-A, Jun 1978.
15. Marhof, J. "The Structural Components of the Intervertebral Disc" The Journal of Bone and Joint Surgery, Vol 56-A: No. 4, p. 675, Jun 1974.
16. Nachemson, AIFL., Schultz, Albert B. and Berhson, Michael H. "Mechanical Properties of Human Lumbar Spine Motion Segments," Spine, Vol 4: No. 1, p. 1, January/February 1979.
17. Virgin, W. J. "Experimental Investigation into the Physical Properties of the Intervertebral Disc." J. Bone and Jt. Surg. 33-B, 607-611, Nov, 1951.
18. White, Augustus A. and Panjabi, Manottar M. "Clinical Biomechanics of the Spine," Philadelphia, T. P. Lippincott Company, 1978.
19. Zienkiewicz, O. C. "The Finite Element Method," (third edition), London: McGraw-Hill Book Company, 1977.
20. Zienkiewicz, O. C., Watson, M. and King, F. P. "A Numerical Method of Visco-Elastic Stress Analysis," Int Journal of Mechanical Science, Vol 10: 807-827, 1968.

Appendix A

Experimental Protocol

Title: Creep Characteristics of Normal and Herniated Intervertebral Joints in the Lumbar Region of the Spine.

Work Unit:

Principal Investigator: David R. Furlong, 2nd Lt, AFIT/EN

Co-Investigators: A. N. Palazotto, Ph.D., AFIT/EN

E. Paul France 1 Lt, BSC

A.1. Objectives: The purpose of this investigation is to obtain information on the influence of the nucleus pulposus on the viscoelastic properties of the intervertebral joint.

A.2. Introduction: Compressive creep tests will be performed on six specimens from the lumbar section of rhesus monkeys. The disc will be partially herniated and the creep test repeated. The disc will then be herniated with a trephine and the load cycle repeated for a third time. Next, both the experimental procedure and numerical analysis will be brought together and further studied in a Master's thesis at the Air Force Institute of Technology.

Lumbar sections from six rhesus monkeys at the L1-L2 level will be used in the experiment. The general plan of the protocol can be broken down into four parts: procedure, equipment and instrumentation, justification of species, and results.

A.3.1. Preparation

1. The following procedure is for the preparation of each specimen and is to be completed before the morning of the compression test.

2. Specimens will be X-rayed in both the anterior and lateral position. These X-rays will be used to establish column condition and for anthropomorphic reference.

3. Each specimen will consist of the intervertebral disc and its two adjacent vertebral centrums. All soft tissue and the posterior processes will be removed from the specimen. The total height of the test specimen will be taken before and after the posterior elements are removed. All height measurements, throughout the experimentation, should be taken in both the anterior/posterior and lateral directions.

4. The area of the superior and inferior exposed surfaces of the specimen will be photographed in order to obtain their areas.

A.3.2. Phase I

1. The specimen will be subjected to a creep test using the equipment and instrumentation section of this protocol. A constant compressive load of 6.80 Kiloponds will be applied for 8 hours followed by 16 hours of recovery after load removal.

2. The data during the load cycle should be taken in the following manner.

60 samples/min.	0-10 min. of load
6 samples/min.	10-20 min. of load
1 sample/min.	1/3- 8 hrs. of load
60 samples/min.	0-10 min. of unload
6 samples/min.	10-20 min. of unload
1 sample/min.	1/3- 8 hrs. of unload

3. In addition, photographs will be taken throughout the load portion of the test and for the first 8 hours of the unload portion at 24 second intervals.

A.3.3. Phase 2

1. During Phase 2, the disc will be partially herniated and the creep test repeated. At the end of the unload cycle in Phase 1, the specimen will be surgically herniated with a 14 gage hypodermic syringe and stored in a saline rich environment at a cold temperature. It is not to be stored in saline solution because the specimen may absorb the saline thus changing the material properties of the disc. When the disc is herniated, the following measurements should be taken. Before and after herniation, the total height of the specimen is to be taken. The volume of fluid removed is also needed.

2. In the load cycle of the partially herniated specimen, data will be gathered as specified in Phase 1.

A.3.4. Phase 3

1. In the last load cycle, the disc will be fully herniated and the creep test repeated. At the end of the load cycle of the previous phase, the specimen is to be surgically herniated with a 5mm trephine and then stored in a saline rich environment. Before and after herniation, the height of the test specimen is to be taken.

2. In the load cycle, the data gathered will be in the same manner as the previous two test cycles.

A.3.5. Phase 4

1. After the second creep test, the specimen will be stored in a saline rich environment for at least 24 hours before dissection.

2. At the time of dissection, the area of the annulus fibrosis and bony endplate is to be measured. In addition, the approximate volume of the nucleus pulposus will be found through geometric techniques.

3. In the final part, measurements of the vertebral centroms will be obtained as needed to formulate the model.

4. The displacement data from each test will be graphed using a specially prepared plotting routine.

5. The time delay photographs will also be studied to determine pitch and torsion of the specimen. Vertebral unit will be photographed to obtain cross-sectional area.

6. When the specimen is cupped, a minimum of dental acrylic is to be used to minimize shear in the vertebral bodies. After attaching the cups, the total height of the specimen is again to be taken.

7. Two pins will be placed on the lateral surface of each vertebral centrum. The pins will be used as a reference for determining pitch and torsion of the specimen during testing.

8. The specimen will then be stored in a cold normal saline rich environment for no longer than two days until tested.

A.4. Equipment and Instrumentation: Intervertebral joint creep tests will be conducted using three specially built chambers. Each chamber is designed to apply a static vertical load to a specimen and measure the resultant strain using LVDT. The load is applied with the specimen in an upright position (superior/inferior) and can be varied by the addition or the removal of lead weights. Using Dana amplifiers, the LVDT signal is processed and becomes a calibrated voltage output. The output from the three LVDTs is sampled and printed on a Silent 700 as a digital readout. The sampling rate is controlled by the operator who has a choice of between 0.01sec and 10.0min rates. The LVDT instrumentation is calibrated and zeroed before and after each test run. For the 24 hr. duration of each experiment all 3 test chambers are humid-

ified using a cool mist generator.

A.5. Justification of Species: In order to obtain meaningful data concerning the mechanical creep characteristics of the human spine, only animals having a musculoskeletal resemblance to man are appropriate for study. Because of the great amount of comparative biomechanical work done with the rhesus monkey and the baboon spinal columns and the availability of excised spines from cadaver specimens of other experiments, it is economically and scientifically prudent to utilize these species.

A.6. Results: The analysis and conclusions of this study will be presented as part of a Master's thesis at the Air Force Institute of Technology.

VITA

Daivd R. Furlong was born in Wiesbaden, Germany on 13 February 1958. He attended Langley High School in McLean, Virginia and graduated in 1975. He then studied Mechanical Engineering at the Georgia Institute of Technology and graduated in 1979 with a Bachelor of Mechanical Engineering. He received his commission in the Air Force in June 1980 and started his study for a Master of Science in Aeronautical Engineering at the Air Force Institute of Technology.

The experimentation involved several distinct phases. First five specimens were excised from the L₁-L₂ level of young adult rhesus monkeys (*Macaca mulatta*). The prepared specimen consisted of the intervertebral joint and the two adjacent vertebral centrums without either the posterior elements or associated soft tissues. The prepared specimen was subjected to a constant compressive load of sixty-seven newtons for eight hours followed by a relaxation time of sixteen hours. The specimens were then subjected to various stages of herniation and the creep tests were repeated after each herniation.

The analysis was also carried out in several phases. First, the experimental data was graphed using a specially prepared plotting routine for the Cyber 750 machine. A mean displacement curve was then obtained for each set of creep tests by averaging the displacement vs. time curve of each test phase. Next, all specimens were dissected and measured to obtain data needed in formulating a finite element model. In the final phase of the analysis, a viscoelastic axisymmetric finite element model was used to quantify the experimental data. A three parameter Kelvin solid was employed in the finite element solution method. The result of this paper will be used to construct a dynamic model of the vertebral column.

Unclassified

SECURITY CLASSIFICATION OF THIS PAGE (When Data Entered)

REPORT DOCUMENTATION PAGE		READ INSTRUCTIONS BEFORE COMPLETING FORM
1. REPORT NUMBER AFIT/GAE/AA/81D-9	2. GOVT ACCESSION NO. AD-A111 097	3. RECIPIENT'S CATALOG NUMBER
4. TITLE (and Subtitle) The Influence of Surgical Herniation on the Viscoelastic Properties of the Intervertebral Disc		5. TYPE OF REPORT & PERIOD COVERED M.S. Thesis
		6. PERFORMING ORG. REPORT NUMBER
7. AUTHOR(s) David R. Furlong 2nd Lt		8. CONTRACT OR GRANT NUMBER(s)
9. PERFORMING ORGANIZATION NAME AND ADDRESS Air Force Institute of Technology (AFIT-CN) Wright-Patterson AFB, Ohio 45433		10. PROGRAM ELEMENT, PROJECT, TASK AREA & WORK UNIT NUMBERS
11. CONTROLLING OFFICE NAME AND ADDRESS		12. REPORT DATE December 1981
		13. NUMBER OF PAGES 85
14. MONITORING AGENCY NAME & ADDRESS (if different from Controlling Office)		15. SECURITY CLASS. (of this report) Unclassified
		15a. DECLASSIFICATION/DOWNGRADING SCHEDULE
16. DISTRIBUTION STATEMENT (of this Report) Approved for public release; distribution unlimited		
17. DISTRIBUTION STATEMENT (of the abstract entered in Block 20, if different from Report) 28 JAN 1982		
18. SUPPLEMENTARY NOTES Approved for public release; IAW AFR 190-17 Fredrick A. Lynch, Major, USAF Director of Public Affairs		
19. KEY WORDS (Continue on reverse side if necessary and identify by block number) Viscoelastic Herniation Material Properties Intervertebral Disc Air Force Institute of Technology (AFIT) Wright-Patterson AFB, OH 45433		
20. ABSTRACT (Continue on reverse side if necessary and identify by block number) In the phenomena of aircraft flight, the body is subjected to forces and stress that are not ordinarily encountered. Examples are emergency egress from an aircraft, high G turns, and random vibrations and disturbances. Anatomically the vertebral column must absorb much of these excesses. In light of these biomechanics problems of flight, this thesis will study the influence of surgical herniation on the viscoelastic properties of the intervertebral joint. The presentation shall be broken down into two phases: experimentation and analysis.		

DD FORM 1473 1 JAN 73 EDITION OF 1 NOV 65 IS OBSOLETE

SECURITY CLASSIFICATION OF THIS PAGE (When Data Entered)

FILMED
8